Computers and Mathematics with Applications 80 (2020) 1964–1984

Contents lists available at ScienceDirect

Computers and Mathematics with Applications

journal homepage: www.elsevier.com/locate/camwa

Monolithic and splitting solution schemes for fully coupled quasi-static thermo-poroelasticity with nonlinear convective transport☆

Mats Kirkesæther Brun [a,*], Elyes Ahmed [b], Inga Berre [c,d], Jan Martin Nordbotten [c], Florin Adrian Radu [c]

[a] CEES, Dept. of Biosciences, University of Oslo, P. O. Box 1066, N-0316 Oslo, Norway
[b] SINTEF, P. O. Box 124, N-0314 Oslo, Norway
[c] Department of Mathematics, University of Bergen, P.O. Box 7800, N-5020 Bergen, Norway
[d] NORCE Norwegian Research Centre AS, Bergen, Norway

ARTICLE INFO

Article history:
Received 21 June 2019
Received in revised form 20 March 2020
Accepted 21 August 2020
Available online 8 September 2020

Keywords:
Quasi-static thermo-poroelasticity
Nonlinear convective transport
Porous media
Fixed-stress splitting iterative coupling
Contraction mapping
Mixed finite elements

ABSTRACT

This paper concerns monolithic and splitting-based iterative procedures for the coupled nonlinear thermo-poroelasticity model problem. The thermo-poroelastic model problem we consider is formulated as a three-field system of PDE's, consisting of an energy balance equation, a mass balance equation and a momentum balance equation, where the primary variables are temperature, fluid pressure, and elastic displacement. Due to the presence of a nonlinear convective transport term in the energy balance equation, it is convenient to have access to both the pressure and temperature gradients. Hence, we introduce these as two additional variables and extend the original three-field model to a five-field model. For the numerical solution of this five-field formulation, we compare six approaches that differ by how we treat the coupling/decoupling between the flow and/from heat and/from the mechanics, suitable for varying coupling strength between the three physical processes. The approaches have in common a simultaneous application of the so-called *L*-scheme, which works both to stabilize iterative splitting as well as to linearize nonlinear problems, and can be seen as a generalization of the Undrained and Fixed-Stress Split algorithms. More precisely, the derived procedures transform a nonlinear and fully coupled problem into a set of simpler subproblems to be solved sequentially in an iterative fashion. We provide a convergence proof for the derived algorithms, and demonstrate their performance through several numerical examples investigating different strengths of the coupling between the different processes.

1. Introduction

1.1. Problem statement

The field of *poroelasticity* aims to describe the interaction between viscous fluid flow and elastic solid deformation within a porous material, and it was pioneered through the works of K. Terzhagi [1] and M. A. Biot [2,3]. In the fully-

☆ This work forms part of Norwegian Research Council project 250223.
* Corresponding author.
E-mail addresses: m.k.brun@ibv.uio.no (M.K. Brun), elyes.ahmed@sintef.no (E. Ahmed), inga.berre@uib.no (I. Berre), jan.nordbotten@uib.no (J.M. Nordbotten), florin.radu@uib.no (F.A. Radu).

https://doi.org/10.1016/j.camwa.2020.08.022

saturated, quasi-static regime, the mathematical modeling of such processes constitutes a coupled two-field linear model where the primary variables are the fluid pressure and the elastic displacement of the solid. This is known as the quasi-static Biot model.

In many important applications, such as geothermal energy extraction, nuclear waste disposal and carbon storage, temperature also plays a vital role and must therefore be included in the aforementioned model. Thus, we consider here a *thermo-poroelastic* system which can be seen as a generalization of the Biot system to the non-isothermal case; i.e., the coupled processes are heat, flow, and geomechanics. Since it is the cornerstone of many complex models, we focus on the following nonlinear and coupled quasi-static thermo-poroelastic equations as described in [4–6]: Find the temperature T, the pressure p, and the displacement $\mathbf{u}$ such that

$$\partial_t \psi(p, \mathbf{u}, T) + c_f(\mathbf{K}\nabla p)\cdot\nabla T - \nabla\cdot(\boldsymbol{\Theta}\nabla T) = z, \quad \text{in } \Omega\times(0,t_f), \tag{1.1a}$$

$$-\nabla\cdot\boldsymbol{\theta}(\mathbf{u}) + \alpha\nabla p + \beta\nabla T = \mathbf{f}, \quad \text{in } \Omega\times(0,t_f), \tag{1.1b}$$

$$\partial_t \varphi(p, T, \mathbf{u}) - \nabla\cdot(\mathbf{K}\nabla p) = g, \quad \text{in } \Omega\times(0,t_f), \tag{1.1c}$$

$$T = 0, \quad \mathbf{u} = 0, \quad p = 0, \quad \text{on } \partial\Omega\times(0,t_f), \tag{1.1d}$$

$$T(\cdot,0) = T_0, \quad \mathbf{u}(\cdot,0) = \mathbf{u}_0, \quad p(\cdot,0) = p_0, \quad \text{in } \Omega. \tag{1.1e}$$

In the above model, Ω is a bounded (connected and open) domain in $\mathbb{R}^d$, $d = 2$ or 3, and $t_f > 0$ is the final time. The function z is the heat source, g is the mass source, and $\mathbf{f}$ is the body force. The functionals ψ and φ denote the heat content and fluid content, respectively; i.e., $\psi(p,\mathbf{u},T) := a_0T - b_0p + \beta\nabla\cdot\mathbf{u}$, and $\varphi(p,\mathbf{u},T) := c_0p - b_0T + \alpha\nabla\cdot\mathbf{u}$, where c_0 is the constrained-specific storage coefficient, a_0 is the effective volumetric heat capacity divided by reference temperature, b_0 is the thermal dilation coefficient, α is the Biot–Willis constant, and β is the thermal stress coefficient. The parameter c_f is the volumetric heat capacity of the fluid divided by reference temperature, $\mathbf{K} = (K_{ij})_{i,j=1}^d$ is the permeability divided by fluid viscosity, and $\boldsymbol{\Theta} = (\Theta_{ij})_{i,j=1}^d$ is the effective thermal conductivity divided by reference temperature. The function $\boldsymbol{\theta}$ denotes the effective stress tensor, i.e., $\boldsymbol{\theta}(\mathbf{u}) := 2\mu\boldsymbol{\varepsilon}(\mathbf{u}) + \lambda\nabla\cdot\mathbf{u}\mathbf{I}$, where $\boldsymbol{\varepsilon}(\mathbf{u}) := (\nabla\mathbf{u} + \nabla\mathbf{u}^\top)/2$ the symmetric part of $\nabla\mathbf{u}$, and $\mathbf{I}$ is the identity tensor. Finally, T_0 is the initial temperature, $\mathbf{u}_0$ is the initial displacement and p_0 is the initial pressure. For the present purposes we consider (1.1a)–(1.1e) to be given in dimensionless form, i.e., coefficients and variables are without units.

Note that the above model introduces a nonlinearity in a coupling term, which is the convective transport term in the energy balance equation (1.1a). The presence of this nonlinear coupling term strongly complicates the problem compared to the isothermal case (i.e., to the linear Biot model). Note that if $b_0 = \beta = 0$, the flow and mechanics decouples from the heat, and Biot's model is recovered. For the derivation of the constitutive equations of thermo-poroelasticity we refer to the works [6–8], and particularly to [4–6] where the above model was derived within the framework of the two-scale asymptotic expansion method (see, e.g., [9] for a review of this technique).

Remark 1.1 (*Boundary Condition*)**.** We present the problem (1.1a)–(1.1e) with homogeneous Dirichlet boundary conditions only to keep the following presentation as concise as possible. Extending to non-homogeneous or Neumann boundary conditions is straightforward. All results presented in the sequel are valid also for Neumann boundary conditions.

1.2. Weak solution and well-posedness of the continuous problem

The common structure of mathematical models that are based on (systems of) scalar conservation laws of the form (1.1a) where nonlinear gradient terms appear suggests introducing the heat flux, $\mathbf{r} := -\boldsymbol{\Theta}\nabla T$, or the Darcy flux, $\mathbf{w} := -\mathbf{K}\nabla p$, as an additional variable. Thus, either the term $c_f(\mathbf{K}\nabla p)\cdot\nabla T$ becomes $\left[-c_f(\mathbf{w}\cdot\nabla T)\right]$ or $\left[-c_f((\mathbf{K}\otimes\boldsymbol{\Theta}^{-1})\mathbf{r}\cdot\nabla p)\right]$, e.g., [10,11]. Precisely, it is well known that such terms, dealing non-linearly with the coupled convection, can be quite difficult to approximate correctly in their actual forms. This altogether leads to challenging numerical issues. Furthermore, the choice to introduce the heat flux or the Darcy flux as a new variable depends strongly on which process (flow or heat) that dominates and may result in a different treatment of the convective term. Here, to avoid some of these complexities, we adopt from [12] the mixed form for both the heat and flow subproblems (1.1a) and (1.1b), keeping in mind that Mixed Finite Element (also Finite Volume) literature has developed techniques to handle convective terms [13,14]. Throughout the paper we consider the following assumptions to hold true:

- (**A1**) $\mathbf{K} : \mathbb{R}^d \to \mathbb{R}^{d\times d}$ is constant in time, symmetric, definite and positive; there exist $k_m > 0$ and k_M such that $k_m|\zeta|^2 \le \zeta^\top\mathbf{K}(x)\zeta$ and $|\mathbf{K}(x)\zeta| \le k_M|\zeta|$, $\forall\zeta\in\mathbb{R}^d\setminus\{0\}$.
- (**A2**) $\boldsymbol{\Theta} : \mathbb{R}^d \to \mathbb{R}^{d\times d}$ is constant in time, symmetric, definite and positive; there exist $\theta_m > 0$ and θ_M such that $\theta_m|\zeta|^2 \le \zeta^\top\boldsymbol{\Theta}(x)\zeta$ and $|\boldsymbol{\Theta}(x)\zeta| \le \theta_M|\zeta|$, $\forall\zeta\in\mathbb{R}^d\setminus\{0\}$.
- (**A3**) The coefficients a_0, b_0, c_0, c_f, α and β are strictly positive constants.
- (**A4**) The coefficients a_0, b_0 and c_0 are such that $c_0 - b_0 > 0$ and $a_0 - b_0 > 0$.
- (**A5**) The source terms are such that $z, g \in L^2(0,t_f;L^2(\Omega))$ and $\mathbf{f}\in H^1(0,t_f;L^2(\Omega))$. Furthermore, z, g and $\mathbf{f}$ are piecewise constant in time with respect to the temporal mesh of Section 2.
- (**A6**) The initial data are such that $p_0, T_0 \in H_0^1(\Omega)$ and $\mathbf{u}_0\in(L^2(\Omega))^d$.

Before transcribing the mixed variational formulation of the problem, we introduce some notations:

$$\mathcal{T} := L^2(\Omega), \quad \mathcal{R} := H(\mathrm{div}, \Omega), \quad \mathcal{P} := L^2(\Omega), \quad \mathcal{W} := H(\mathrm{div}, \Omega), \quad \mathcal{U} := (L^2(\Omega))^d,$$

where we denote by $(\cdot, \cdot)$ the standard $L^2(\Omega)$ inner product, and by $\|\cdot\|$ the induced $L^2(\Omega)$ norm. Due to (**A1**) and (**A2**), the tensors $\mathbf{K}$ and $\boldsymbol{\Theta}$ (and their inverses) define $L^2(\Omega)$-equivalent norms, which we denote by $\|\mathbf{v}\|_{\mathbf{K}} := (\mathbf{K}\mathbf{v}, \mathbf{v})^{1/2}$ (and $\|\mathbf{v}\|_{\mathbf{K}^{-1}} := (\mathbf{K}^{-1}\mathbf{v}, \mathbf{v})^{1/2}$), and similarly with $\boldsymbol{\Theta}$. With this, we define the variational formulation of (1.1a)–(1.1d) as follows:

Definition 1.1 (*The Continuous Formulation [12]*)**.** Assuming (**A1**)–(**A6**) hold true, the fully coupled mixed-primal formulation of (1.1) reads:

Find $(T(t), \mathbf{r}(t), p(t), \mathbf{w}(t), \mathbf{u}(t)) \in \mathcal{T} \times \mathcal{R} \times \mathcal{P} \times \mathcal{W} \times \mathcal{U}$, such that for a.e. $t \in (0, t_f)$

$$(\partial_t \psi(p, T, \mathbf{u}), S) + c_f(\mathbf{w} \cdot \boldsymbol{\Theta}^{-1}\mathbf{r}, S) + (\nabla \cdot \mathbf{r}, S) = (z, S), \quad \forall S \in \mathcal{T}, \tag{1.2a}$$

$$(\boldsymbol{\Theta}^{-1}\mathbf{r}, \mathbf{y}) - (T, \nabla \cdot \mathbf{y}) = 0, \quad \forall \mathbf{y} \in \mathcal{R}, \tag{1.2b}$$

$$(\partial_t \varphi(p, T, \mathbf{u}), q) + (\nabla \cdot \mathbf{w}, q) = (g, q), \quad \forall q \in \mathcal{P}, \tag{1.2c}$$

$$(\mathbf{K}^{-1}\mathbf{w}, \mathbf{z}) - (p, \nabla \cdot \mathbf{z}) = 0, \quad \forall \mathbf{z} \in \mathcal{W}, \tag{1.2d}$$

$$(\boldsymbol{\theta}(\mathbf{u}), \boldsymbol{\varepsilon}(\mathbf{v})) - (\beta T + \alpha p, \nabla \cdot \mathbf{v}) = (\mathbf{f}, \mathbf{v}), \quad \forall \mathbf{v} \in \mathcal{U}, \tag{1.2e}$$

together with the initial conditions (1.1e).

The above variational problem was analyzed in [12]. There, it was shown that under the assumption that the heat flux (or Darcy flux) is such that $\mathbf{r}(t) \in (L^\infty(\Omega))^d$, for $t \in (0, t_f)$, the problem (1.2) has a unique weak solution. Moreover, it was shown that with additional regularity on the data, i.e., $\mathbf{f} \in H^2\left(0, t_f; (L^2(\Omega))^d\right)$, $h, g \in H^1(0, t_f; L^2(\Omega))$, and $T_0, p_0 \in H_0^1(\Omega) \cap H^2(\Omega)$, the fluxes are bounded functions. We also note that in [12] constraints on the parameters similar to (**A4**) were needed for the well-posedness of the above variational problem.

1.3. Goal and positioning of the paper

The simulation of thermo-poroelasticity problems is challenging due to the coexistence of different physics which necessitates a coupled set of equations. For these types of problems, there are typically three different approaches employed in modeling fluid flow coupled with reservoir geomechanics. They are known as the fully implicit, the explicit (loosely or weakly) coupling, and the *splitting-iterative* approaches. The main problem for the applicability of the fully implicit approach, which solves simultaneously the above *three-processes* (flow, heat and mechanics) problem, is that it results in a very large discrete system of equations to be solved at each time step. Moreover, it does not facilitate the (re-)use of existing codes dedicated to the various subproblems. On the other hand, the fully coupled approach has excellent stability properties [15,16]. An alternative is a weakly coupled approach, which results in a smaller discrete system and a lower computational cost compared to the fully implicit (monolithic) approach. On the other hand, accuracy may be sacrificed, and the sequential approach is only conditionally stable [17,18]. Herein, we adopt an iterative coupling approach, which provides a compromise between the implicit and explicit: At each iteration it has the cost of the sequential approach, yet it converges to the fully coupled implicit approach. We implement the idea of iterative coupling by resolving iteratively the two/three subsystems (depending on the choice of splitting procedure) and by exchanging the values of the shared state variables in an iterative fashion using a general framework of linearly stabilized schemes [19,20].

We argue that adopting an iterative method for the *nonlinear and fully coupled three-processes* problem, can be considered almost essential for efficient simulation, since the fully coupled approach leads to a prohibitively large system (particularly if MFE methods are adopted [15,21–23]), incorporating different equations that are varied in type and with nonlinearities. The advantage of the iterative approaches considered in this paper is that, at each iteration, smaller, easier-to-solve systems are coupled iteratively through algorithms [22,24]. Another advantage that distinguishes our approaches is the possibility of *reusing existing codes* for different numerical schemes and coupling techniques specialized to each component of the problem (see e.g., [25,26]). For classical linear poroelasticity, the iterative coupling procedures mentioned above has been studied extensively [19,20,27–33]. In particular, two such algorithms have received considerable attention: The “Undrained Split”(constant fluid mass during structure deformation) and the “Fixed Stress Split”(constant volumetric mean total stress during solution of flow problem). In [30], these were first shown to be unconditionally stable. In [20,32] contraction estimates and rates of convergence were derived.

The Undrained Split/Fixed Stress Split algorithms have been generalized in the context of the so-called *L-schemes*. In the context of coupled problems, these schemes involve adding an artificial stabilization term to one or more of the subproblems with a parameter $L > 0$. Here, the quantity held constant while solving of one of the subproblems needs not have any physical interpretation. In this sense, the L-scheme generalizes the Undrained Split/Fixed Stress Split algorithms and, due to the removal of physical constraints on the stabilization terms, allows for further optimization. The L-scheme can also be employed as a linearization procedure for nonlinear problems, with the parameter $L > 0$ mimicking the Jacobian from Newton iteration. To determine the parameter $L > 0$ for any given problem, derived convergence estimates are necessary. The L-scheme has been shown to perform robustly for Richards equation [34,35], for both linear

and nonlinear coupled flow and geomechanics [19,36], for unsaturated/variably saturated porous media [37,38], for two-phase flow [39], and for nonlinear diffusion problems [40]. In this paper, we utilize the L-scheme framework both as a decoupling strategy and as a linearization method.

Although the literature on iterative coupling procedures for (isothermal) poroelastic problems is quite extensive, thermo-poroelastic problems have not received the same amount of attention. Sequential iterative methods for linear thermo-poroelasticity were considered in [41]. Iterative splitting schemes for separate poroelasticity and thermoelasticity problems were considered in [42]. Compared to problems of (two-field) coupled flow and mechanics (which can be solved either sequentially or monolithically) we now have additional options in terms of partial decoupling, i.e., solving two of the subproblems together decoupled from the third. Combinatorially, this yields six variations of iterative procedures, ranging from monolithic to fully decoupled. In this work, we focus on the algorithmic developments necessary to handle the nonlinear coupling structure of the problem and propose and analyze all six iterative algorithms for nonlinear thermo-poroelasticity. In particular, we employ variations of the L-scheme in all six algorithms, with artificial stabilization terms added to both the flow and heat subproblems. By proving a contraction of all schemes, we obtain explicit expressions for the linearization parameters that guarantee the stability and convergence of all schemes. The main *advantage* of the L-scheme is that it treats simultaneously the coupling and the non-linearity effects. Thus, no inner iterative approaches are required; see e.g., [43] where L-scheme type approaches are developed to treat iteratively a combined domain decomposition and nonlinearity problem. In most cases, the convergence is linear in the required energy norms. Furthermore, the necessary constraint on the time step is not severe.

The reason we propose six algorithms is the following: The coupling strength of the heat, flow and mechanics may vary depending on the physics at hand. Moreover, the practitioner may have access to existing software of various capabilities. Precisely, to develop robust and efficient solution procedures for the *three-processes problem* at hand, one should *in principle* take into account which process (*the mechanics* and/or *flow* and/or *heat flow*) dominate the full problem. In practice, one must also take into account implementation time and available frameworks. Thus, to be agnostic towards the dominating processes and other real-world constraints, we derive a complete framework for this model problem. The six variations of iterative coupling/decoupling algorithms for thermo-poroelasticity cover all possibilities of varying coupling strength between the three physical processes involved. Note that the developed algorithms are applicable on any numerical schemes used to obtain the solutions of the different processes [44,45]. For the convergence analysis, we derive energy-type estimates from which we infer the convergence of the iterate solutions as well as obtaining strict lower bounds on the stabilization parameters, and an upper bound on the time step. A "cut-off"operator $\mathcal{M}$ is introduced in the mixed setting in order to make the iterative schemes converge, but we emphasize that this does not affect the model in practice. Several numerical tests validate our proposed algorithms. In particular, we show that by using the derived stabilization estimates, the proposed algorithms perform robustly with respect to both mesh refinement and a wide range of different problem parameters.

The article is organized as follows: In Section 2 we present the fully discrete formulation of the thermo-poroelastic model, and in Section 3 we present all six iterative algorithms. In Section 4, convergence analysis based on contraction estimates is derived, from which the well-posedness of the discrete scheme is inferred in addition to the bounds on the stabilization parameters and time step. In Section 5 we provide several numerical experiments, and finally in Section 6 some concluding remarks.

2. Discrete setting

Let $\mathcal{X}_h$ be a simplicial mesh of Ω, matching in the sense that for two distinct elements of $\mathcal{X}_h$ their intersection is either an empty set or their common vertex or edge. Let h_K denote the diameter of $K \in \mathcal{X}_h$ and let h be the largest diameter of all such triangles, i.e., $h := \max_{K\in\mathcal{X}_h} h_K$. For the time partition, we let $\{t^n : n = 0, 1, \ldots, N\}$ be the discrete time steps, where $0 := t^0 < t^1 < \cdots < t^N = t_f$, and let $\tau^n = t^n - t^{n-1}$, $n \geq 1$, be the difference between consecutive discrete times. In other words, we have $t^n := \sum_{\ell=1}^{n} \tau^\ell$, $1 \leq n \leq N$, and therefrom $t_f = \sum_{n=1}^{N} \tau^n$.

For the discrete spaces, we let $\mathcal{T}_h$, $\mathcal{R}_h$, $\mathcal{P}_h$, $\mathcal{W}_h$ and $\mathcal{U}_h$ be suitable finite element spaces corresponding to the infinite dimensional spaces of Section 1.2, where we assume that

$$\operatorname{div} \mathcal{R}_h = \mathcal{T}_h \quad \text{and} \quad \operatorname{div} \mathcal{W}_h = \mathcal{P}_h. \tag{2.1}$$

For the time discretization we employ a backward Euler scheme. For the sake of simplicity, we take the source terms $\mathbf{f}$, g and z to be piecewise constant in time. We denote by $(T_h^n, \mathbf{r}_h^n, p_h^n, \mathbf{w}_h^n, \mathbf{u}_h^n)$ the discrete counterpart of the solution tuple to problem (1.2) at time t^n.

Before giving the discrete version of the variational formulation (1.2a)–(1.2e), we need to introduce the so-called cut-off operator $\mathcal{M}$ as described in e.g., [10,11] as

$$\mathcal{M}(\mathbf{z})(x) := \begin{cases} \mathbf{z}(x), & |\mathbf{z}(x)| \leq M, \\ M\mathbf{z}(x)/|\mathbf{z}(x)|, & |\mathbf{z}(x)| > M, \end{cases} \tag{2.2}$$

where M is a (large) positive constant. We note that the introduction of this operator in the following discrete variational formulation has little or no practical implications, but is necessary in order to facilitate the convergence analysis. Obviously, if the exact fluxes are bounded, i.e., $\mathbf{w}^n, \mathbf{r}^n \in (L^\infty(\Omega))^d$, and if we pick M large enough, we have $\mathcal{M}(\mathbf{w}^n)(x) = \mathbf{w}^n(x)$ and $\mathcal{M}(\mathbf{r}^n)(x) = \mathbf{r}^n(x)$. Thus, a precise value for the constant M is not necessary.

Definition 2.1 (*The Coupled mixed × mixed and Galerkin Finite Element Scheme*)**.** The discrete formulation of the problem (1.2) reads: Given $\psi(p_h^0, T_h^0, \mathbf{u}_h^0)$ and $\varphi(p_h^0, T_h^0, \mathbf{u}_h^0)$, then, for $n = 1, \ldots, N$, find $(T_h^n, \mathbf{r}_h^n, p_h^n, \mathbf{w}_h^n, \mathbf{u}_h^n) \in \mathcal{T}_h \times \mathcal{R}_h \times \mathcal{P}_h \times \mathcal{W}_h \times \mathcal{U}_h$ such that

$$
\begin{aligned}
&(\psi(p_h^n, T_h^n, \mathbf{u}_h^n), S_h) + \tau^n c_f(\mathcal{M}(\mathbf{w}_h^n) \cdot \boldsymbol{\Theta}^{-1}\mathcal{M}(\mathbf{r}_h^n), S_h) + \tau^n(\nabla \cdot \mathbf{r}_h^n, S_h) \\
&\qquad = \tau^n(z^n, S_h) + (\psi(p_h^{n-1}, T_h^{n-1}, \mathbf{u}_h^{n-1}), S_h), \qquad \forall S_h \in \mathcal{T}_h, \qquad (2.3a)\\
&(\boldsymbol{\Theta}^{-1}\mathbf{r}_h^n, \mathbf{y}_h) - (T_h^n, \nabla \cdot \mathbf{y}_h) = 0, \qquad \forall \mathbf{y}_h \in \mathcal{R}_h, \qquad (2.3b)\\
&(\varphi(p_h^n, T_h^n, \mathbf{u}_h^n), q_h) + \tau^n(\nabla \cdot \mathbf{w}_h^n, q_h) \\
&\qquad = \tau^n(g^n, q_h) + (\psi(p_h^{n-1}, T_h^{n-1}, \mathbf{u}_h^{n-1}), q_h), \qquad \forall q_h \in \mathcal{P}_h, \qquad (2.3c)\\
&(\mathbf{K}^{-1}\mathbf{w}_h^n, \mathbf{z}_h) - (p_h^n, \nabla \cdot \mathbf{z}_h) = 0, \qquad \forall \mathbf{z}_h \in \mathcal{W}_h, \qquad (2.3d)\\
&2\mu(\boldsymbol{\varepsilon}(\mathbf{u}_h^n), \boldsymbol{\varepsilon}(\mathbf{v}_h)) + \lambda(\nabla \cdot \mathbf{u}_h^n, \nabla \cdot \mathbf{v}_h) \\
&\qquad - (\beta T_h^n + \alpha p_h^n, \nabla \cdot \mathbf{v}_h) = (\mathbf{f}^n, \mathbf{v}_h), \qquad \forall \mathbf{v}_h \in \mathcal{U}_h. \qquad (2.3e)
\end{aligned}
$$

In the above scheme, we used $(\mathcal{M}(\mathbf{w}_h^n) \cdot \boldsymbol{\Theta}^{-1}\mathcal{M}(\mathbf{r}_h^n), S_h)$ for the approximation of the convective coupling term instead of the original $(\mathbf{w}_h^n \cdot \boldsymbol{\Theta}^{-1}\mathbf{r}_h^n, S_h)$. The reason for this approximation will be clarified later. Eqs. (2.3a)–(2.3b) form the discrete mixed scheme of the *heat subproblem*, (2.3c)–(2.3d) form the discrete mixed scheme for the *flow subproblem*, and (2.3e) is the discrete form of the *mechanics subproblem* with the Galerkin finite element method. Together, these subproblems make up the nonlinear and fully coupled discrete version of the *thermo-poroelastic problem*. In the next section, their iterative solution procedure is detailed.

Remark 2.1 (*Convective Coupling Term*)**.** The convective coupling term $(\mathbf{w}_h^n \cdot \boldsymbol{\Theta}^{-1}\mathbf{r}_h^n, S_h)$ can also be approximated by $(\mathcal{M}(\mathbf{w}_h^n) \cdot \boldsymbol{\Theta}^{-1}\mathcal{R}(\mathbf{r}_h^n), S_h)$, where two different cut-off operators, $\mathcal{M}$ and $\mathcal{R}$ are used (defined with different constants M and R, respectively). In that case, the underlying iterative methods of Section 3 as well as the convergence analysis of Section 4 remains true with minor modifications in the proofs. For simplicity, we let $\mathcal{M} = \mathcal{R}$ (and thus $M = R$).

Remark 2.2 (*Existence of M*)**.** It was shown in [46] for a related poroelastic model that if the flux is bounded on the continuous level, then the discretized flux will inherit this property. Thus, with sufficient regularity of the domain, source and initial data, the existence of the constant M is guaranteed.

3. The *L*-type iterative schemes

We now present six iterative (splitting) algorithms for the discrete thermo-poroelastic problem (2.3). These algorithms involve either decoupling all the subproblems and solving each separately at every iteration (three-step algorithm), or decoupling only one subproblem from the other two which are then solved together (two-step algorithm), or solving a linearized problem monolithically at every iteration (one-step algorithm). We use the letters **H** (Heat), **F** (Flow), and **M** (Mechanics), to abbreviate the algorithms, e.g., a two-step algorithm where the heat and flow subproblems are solved together decoupled from the mechanics subproblem is referred to as (**HF-M**) and similarly for other combinations of coupling/decoupling of the subproblems. Throughout the rest of the article we will mostly refer to the discrete problems and therefore omit the h-subscript on the variables and test functions for cleaner notation. We shall also denote the time step simply by τ, keeping in mind it may depend on n.

At the time step $n \geq 1$, let $(T^{n-1}, \mathbf{r}^{n-1}, p^{n-1}, \mathbf{w}^{n-1}, \mathbf{u}^{n-1})$ be given. We then approximate the solution at the actual time step $n \in \{1, \ldots, N\}$ using the sequence $(T^{n,k}, \mathbf{r}^{n,k}, p^{n,k}, \mathbf{w}^{n,k}, \mathbf{u}^{n,k})$ for $k \geq 0$, defined in an iterative fashion, and where the iterate $(T^{n,0}, \mathbf{r}^{n,0}, p^{n,0}, \mathbf{w}^{n,0}, \mathbf{u}^{n,0})$ is an initial guess (e.g., the solutions at the previous time step). All the algorithms involve adding the stabilization terms $L_T(T^{n,k} - T^{n,k-1}, S)$ and $L_p(p^{n,k} - p^{n,k-1}, q)$ to the left hand sides of Eqs. (2.3a) and (2.3c), respectively, where $L_T, L_p > 0$ are the stabilization parameters (to be chosen later). Furthermore, to make the notation easier, we introduce the parametrized fluid and heat content functionals: For a given $L_T, L_p > 0$, we define

$$
\begin{aligned}
\psi_{L_T}(p, \mathbf{u}, T) &:= (a_0 + L_T)T - b_0 p + \beta \nabla \cdot \mathbf{u}, \qquad (3.1a)\\
\varphi_{L_p}(p, \mathbf{u}, T) &:= (c_0 + L_p)p - b_0 T + \alpha \nabla \cdot \mathbf{u}. \qquad (3.1b)
\end{aligned}
$$

We are now able to present our six iterative algorithms:

3.1. The monolithic scheme (HFM)

At the each iteration $k \geq 1$ of the L-type monolithic scheme, we solve the linearized thermo-poroelastic problem: Given $(T^{n,k-1}, p^{n,k-1}, \mathbf{w}^{n,k-1})$, find $(T^{n,k}, \mathbf{r}^{n,k}, p^{n,k}, \mathbf{w}^{n,k}, \mathbf{u}^{n,k})$ such that

$$
\begin{aligned}
&(\psi_{L_T}(T^{n,k}, p^{n,k}, \mathbf{u}^{n,k}), S) \\
&\quad + \tau c_f(\mathcal{M}(\mathbf{w}^{n,k-1}) \cdot \boldsymbol{\Theta}^{-1}\mathcal{M}(\mathbf{r}^{n,k}), S) + \tau(\nabla \cdot \mathbf{r}^{n,k}, S)
\end{aligned}
$$

$$
\begin{aligned}
&= \tau(z^n, S) + (\psi(T^{n-1}, p^{n-1}, \mathbf{u}^{n-1}), S) \\
&\quad + L_T(T^{n,k-1}, S), && \forall S \in \mathcal{T}_h, && (3.2a)\\
&(\boldsymbol{\Theta}^{-1}\mathbf{r}^{n,k}, \mathbf{y}) - (T^{n,k}, \nabla\cdot\mathbf{y}) = 0, && \forall \mathbf{y} \in \mathcal{R}_h, && (3.2b)\\
&(\varphi_{L_p}(T^{n,k}, p^{n,k}, \mathbf{u}^{n,k}), q) + \tau(\nabla\cdot\mathbf{w}^{n,k}, q) \\
&\quad = \tau(g^n, q) + (\varphi(T^{n-1}, p^{n-1}, \mathbf{u}^{n-1}), q) \\
&\quad + L_p(p^{n,k-1}, q), && \forall q \in \mathcal{P}_h, && (3.2c)\\
&(\mathbf{K}^{-1}\mathbf{w}^{n,k}, \mathbf{z}) - (p^{n,k}, \nabla\cdot\mathbf{z}) = 0, && \forall \mathbf{z} \in \mathcal{W}_h, && (3.2d)\\
&2\mu(\boldsymbol{\varepsilon}(\mathbf{u}^{n,k}), \boldsymbol{\varepsilon}(\mathbf{v})) \\
&\quad + \lambda(\nabla\cdot\mathbf{u}^{n,k}, \nabla\cdot\mathbf{v}) \\
&\quad = (\mathbf{f}^n, \mathbf{v}) + (\beta T^{n,k} + \alpha p^{n,k}, \nabla\cdot\mathbf{v}), && \forall \mathbf{v} \in \mathcal{U}_h. && (3.2e)
\end{aligned}
$$

This algorithm is continued until a fixed tolerance is reached. Clearly, in the above algorithm, the *L*-scheme acts only as a linearization procedure, where we approximate the convective transport term by $\mathcal{M}(\mathbf{w}^{n,k-1})\cdot\boldsymbol{\Theta}^{-1}\mathcal{M}(\mathbf{r}^{n,k})$. One can also approximate this term by $\mathcal{M}(\mathbf{w}^{n,k})\cdot\boldsymbol{\Theta}^{-1}\mathcal{M}(\mathbf{r}^{n,k-1})$, the analysis presented next remains true and follows exactly the same lines. The complexity in this algorithm is that it requires solving a large system generated by (3.2), which combines equations varied in type, and this at each iteration $k \geq 1$. This encourages the development of efficient techniques for the resolution of these coupled systems.

3.2. The partially decoupled schemes

In the second set of iterative schemes, we only decouple the flow (**F**), mechanics (**M**) or heat (**H**) from the remaining two processes, which are being solved monolithically. Thus, we transform the monolithic solver (**HFM**) into a *two-level* iterative approach in which two simpler subproblems are solved sequentially. For the partially and fully decoupled schemes, we do not consider cyclical permutations of the order in which the subproblems are solved to yield different algorithms. The partially decoupled setting delivers the following three iterative approaches:

3.2.1. (HF-M): Coupled heat and flow

Decoupling the mechanics calculation from the coupled flow and heat flow calculation, the first *two-level* iterative scheme reads as follows: At the iteration $k \geq 1$, do:

- **Step 1**: Given $(T^{n,k-1}, p^{n,k-1}, \mathbf{w}^{n,k-1}, \mathbf{u}^{n,k-1})$, find $(T^{n,k}, \mathbf{r}^{n,k}, p^{n,k}, \mathbf{w}^{n,k})$ such that

$$
\begin{aligned}
&(\psi_{L_T}(T^{n,k}, p^{n,k}, \mathbf{u}^{n,k-1}), S) \\
&\quad + \tau c_f(\mathcal{M}(\mathbf{w}^{n,k-1})\cdot\boldsymbol{\Theta}^{-1}\mathcal{M}(\mathbf{r}^{n,k}), S) + \tau(\nabla\cdot\mathbf{r}^{n,k}, S) \\
&\quad = \tau(z^n, S) + (\psi(T^{n-1}, p^{n-1}, \mathbf{u}^{n-1}), S) \\
&\quad + L_T(T^{n,k-1}, S), && \forall S \in \mathcal{T}_h, && (3.3a)\\
&(\boldsymbol{\Theta}^{-1}\mathbf{r}^{n,k}, \mathbf{y}) - (T^{n,k}, \nabla\cdot\mathbf{y}) = 0, && \forall \mathbf{y} \in \mathcal{R}_h, && (3.3b)\\
&(\varphi_{L_p}(T^{n,k}, p^{n,k}, \mathbf{u}^{n,k-1}), q) + \tau(\nabla\cdot\mathbf{w}^{n,k}, q) \\
&\quad = \tau(g^n, q) + (\varphi(T^{n-1}, p^{n-1}, \mathbf{u}^{n-1}), q) \\
&\quad + L_p(p^{n,k-1}, q), && \forall q \in \mathcal{P}_h, && (3.3c)\\
&(\mathbf{K}^{-1}\mathbf{w}^{n,k}, \mathbf{z}) - (p^{n,k}, \nabla\cdot\mathbf{z}) = 0, && \forall \mathbf{z} \in \mathcal{W}_h. && (3.3d)
\end{aligned}
$$

- **Step 2**: Given $(p^{n,k}, T^{n,k})$, find the displacement $\mathbf{u}^{n,k}$ such that

$$
\begin{aligned}
&2\mu(\boldsymbol{\varepsilon}(\mathbf{u}^{n,k}), \boldsymbol{\varepsilon}(\mathbf{v})) \\
&\quad + \lambda(\nabla\cdot\mathbf{u}^{n,k}, \nabla\cdot\mathbf{v}) \\
&\quad = (\mathbf{f}^n, \mathbf{v}) + (\beta T^{n,k} + \alpha p^{n,k}, \nabla\cdot\mathbf{v}), && \forall \mathbf{v} \in \mathcal{U}_h. && (3.3e)
\end{aligned}
$$

3.2.2. (HM-F): Coupled heat and mechanics

The second scheme in this subsection is obtained by decoupling the flow calculation from the remaining coupled thermo-elasticity calculation. This iterative scheme reads: At the iteration $k \geq 1$, do:

- **Step 1**: Given $(T^{n,k-1}, p^{n,k-1}, \mathbf{w}^{n,k-1})$, find $(T^{n,k}, \mathbf{r}^{n,k}, \mathbf{u}^{n,k})$ such that

$$
\begin{aligned}
&(\psi_{L_T}(T^{n,k}, p^{n,k-1}, \mathbf{u}^{n,k}), S) \\
&\quad + \tau c_f(\mathcal{M}(\mathbf{w}^{n,k-1})\cdot\boldsymbol{\Theta}^{-1}\mathcal{M}(\mathbf{r}^{n,k}), S) + \tau(\nabla\cdot\mathbf{r}^{n,k}, S)
\end{aligned}
$$

$$
\begin{aligned}
&= \tau(z^n, S) + (\psi(T^{n-1}, p^{n-1}, \mathbf{u}^{n-1}), S) \\
&\quad + L_T(T^{n,k-1}, S), && \forall S \in \mathcal{T}_h, && (3.4a)\\
&(\boldsymbol{\Theta}^{-1}\mathbf{r}^{n,k}, \mathbf{y}) - (T^{n,k}, \nabla\cdot\mathbf{y}) = 0, && \forall \mathbf{y} \in \mathcal{R}_h, && (3.4b)\\
&2\mu(\boldsymbol{\varepsilon}(\mathbf{u}^{n,k}), \boldsymbol{\varepsilon}(\mathbf{v})) \\
&\quad + \lambda(\nabla\cdot\mathbf{u}^{n,k}, \nabla\cdot\mathbf{v}) \\
&\quad - \beta(T^{n,k}, \nabla\cdot\mathbf{v}) = (\mathbf{f}^n, \mathbf{v}) + \alpha(p^{n,k-1}, \nabla\cdot\mathbf{v}), && \forall \mathbf{v} \in \mathcal{U}_h. && (3.4c)
\end{aligned}
$$

• **Step 2**: Given $(T^{n,k}, \mathbf{u}^{n,k}, p^{n,k-1})$, find $(p^{n,k}, \mathbf{w}^{n,k})$ such that

$$
\begin{aligned}
&(c_0 + L_p)(p^{n,k}, q) + \tau(\nabla\cdot\mathbf{w}^{n,k}, q) \\
&\quad = \tau(g^n, q) + (\varphi(T^{n-1}, p^{n-1}, \mathbf{u}^{n-1}), q) \\
&\quad + L_p(p^{n,k-1}, q) + b_0(T^{n,k}, q) - \alpha(\nabla\cdot\mathbf{u}^{n,k}, q), && \forall q \in \mathcal{P}_h, && (3.4d)\\
&(\mathbf{K}^{-1}\mathbf{w}^{n,k}, \mathbf{z}) - (p^{n,k}, \nabla\cdot\mathbf{z}) = 0, && \forall \mathbf{z} \in \mathcal{W}_h. && (3.4e)
\end{aligned}
$$

3.2.3. (FM-H): Coupled flow and mechanics

The last *two-level* scheme is obtained by decoupling the poro-elasticity calculation (solved monolithically) from the heat flow. Note that a similar scheme was proposed in [47] for two-phase flow. This iterative scheme reads: At the iteration $k \geq 1$, do:

• **Step 1**: Given $(p^{n,k-1}, \mathbf{u}^{n,k-1}, T^{n,k-1})$, find $(p^{n,k}, \mathbf{w}^{n,k}, \mathbf{u}^{n,k})$ such that

$$
\begin{aligned}
&(\varphi_{L_p}(T^{n,k-1}, p^{n,k}, \mathbf{u}^{n,k}), q) + \tau(\nabla\cdot\mathbf{w}^{n,k}, q) \\
&\quad = \tau(g^n, q) + (\varphi(T^{n-1}, p^{n-1}, \mathbf{u}^{n-1}), q) \\
&\quad + L_p(p^{n,k-1}, q), && \forall q \in \mathcal{P}_h, && (3.5a)\\
&(\mathbf{K}^{-1}\mathbf{w}^{n,k}, \mathbf{z}) - (p^{n,k}, \nabla\cdot\mathbf{z}) = 0, && \forall \mathbf{z} \in \mathcal{W}_h, && (3.5b)\\
&2\mu(\boldsymbol{\varepsilon}(\mathbf{u}^{n,k}), \boldsymbol{\varepsilon}(\mathbf{v})) \\
&\quad + \lambda(\nabla\cdot\mathbf{u}^{n,k}, \nabla\cdot\mathbf{v}) - \alpha(p^{n,k}, \nabla\cdot\mathbf{v}) \\
&\quad = (\mathbf{f}^n, \mathbf{v}) + \beta(T^{n,k-1}, \nabla\cdot\mathbf{v}), && \forall \mathbf{v} \in \mathcal{U}_h. && (3.5c)
\end{aligned}
$$

• **Step 2**: Given $(p^{n,k}, \mathbf{w}^{n,k}, \mathbf{u}^{n,k}, T^{n,k-1})$, find $(T^{n,k}, \mathbf{r}^{n,k})$ such that

$$
\begin{aligned}
&(a_0 + L_T)(T^{n,k}, S) \\
&\quad + \tau c_f(\mathcal{M}(\mathbf{w}^{n,k})\cdot\boldsymbol{\Theta}^{-1}\mathcal{M}(\mathbf{r}^{n,k}), S) + \tau(\nabla\cdot\mathbf{r}^{n,k}, S) \\
&\quad = \tau(z^n, S) + (\psi(T^{n-1}, p^{n-1}, \mathbf{u}^{n-1}), S) \\
&\quad + L_T(T^{n,k-1}, S) + b_0(p^{n,k}, S) - \beta(\nabla\cdot\mathbf{u}^{n,k}, S), && \forall S \in \mathcal{T}_h, && (3.5d)\\
&(\boldsymbol{\Theta}^{-1}\mathbf{r}^{n,k}, \mathbf{y}) - (T^{n,k}, \nabla\cdot\mathbf{y}) = 0, && \forall \mathbf{y} \in \mathcal{R}_h. && (3.5e)
\end{aligned}
$$

3.3. The fully decoupled schemes

In this set of iterative coupling schemes, we simply split the three processes, providing three subproblems to be solved sequentially. Fixing the mechanics calculation in the third level, two approaches are then derived in which either the problem of flow or heat transfer is solved first followed by solving the other system and then the mechanics using the already calculated information. These schemes lead to solving much simpler subsystems through the algorithm. In addition, they enable the reuse of existing codes for each component of the problem.

3.3.1. (H-F-M): Decoupled heat–flow–mechanics

At each iteration all three subproblems are decoupled, and are solved in the order heat → flow → mechanics. This iterative scheme reads: At the iteration $k \geq 1$, do:

• **Step 1**: Given $(p^{n,k-1}, \mathbf{w}^{n,k-1}, T^{n,k-1}, \mathbf{u}^{n,k-1})$ find $(T^{n,k}, \mathbf{r}^{n,k})$ such that

$$
\begin{aligned}
&(\psi_{L_T}(T^{n,k}, p^{n,k-1}, \mathbf{u}^{n,k-1}), S) \\
&\quad + \tau c_f(\mathcal{M}(\mathbf{w}^{n,k-1})\cdot\boldsymbol{\Theta}^{-1}\mathcal{M}(\mathbf{r}^{n,k}), S) + \tau(\nabla\cdot\mathbf{r}^{n,k}, S) \\
&\quad = \tau(z^n, S) + (\psi(T^{n-1}, p^{n-1}, \mathbf{u}^{n-1}), S) \\
&\quad + L_T(T^{n,k-1}, S), && \forall S \in \mathcal{T}_h, && (3.6a)\\
&(\boldsymbol{\Theta}^{-1}\mathbf{r}^{n,k}, \mathbf{y}) - (T^{n,k}, \nabla\cdot\mathbf{y}) = 0, && \forall \mathbf{y} \in \mathcal{R}_h. && (3.6b)
\end{aligned}
$$

• **Step 2**: Given $(p^{n,k-1}, T^{n,k}, \mathbf{u}^{n,k-1})$ find $(p^{n,k}, \mathbf{w}^{n,k})$ such that

$$\begin{aligned}&(\varphi_{L_p}(T^{n,k}, p^{n,k}, \mathbf{u}^{n,k}), q) + \tau(\nabla \cdot \mathbf{w}^{n,k}, q)\\ &\quad = \tau(g, q) + (\varphi(T^{n-1}, p^{n-1}, \mathbf{u}^{n-1}), q)\\ &\qquad + L_p(p^{n,k-1}, q) + b_0(T^{n,k}, q) - \alpha(\nabla \cdot \mathbf{u}^{n,k-1}, q), \qquad \forall q \in \mathcal{P}_h, \end{aligned} \tag{3.6c}$$

$$(\mathbf{K}^{-1}\mathbf{w}^{n,k}, \mathbf{z}) - (p^{n,k}, \nabla \cdot \mathbf{z}) = 0, \qquad \forall \mathbf{z} \in \mathcal{W}_h. \tag{3.6d}$$

• **Step 3**: Given $(p^{n,k}, T^{n,k})$ find $\mathbf{u}^{n,k}$ such that

$$\begin{aligned}&2\mu(\boldsymbol{\varepsilon}(\mathbf{u}^{n,k}), \boldsymbol{\varepsilon}(\mathbf{v})) + \lambda(\nabla \cdot \mathbf{u}^{n,k}, \nabla \cdot \mathbf{v})\\ &\quad = (\mathbf{f}, \mathbf{v}) + (\beta T^{n,k} + \alpha p^{n,k}, \nabla \cdot \mathbf{v}), \qquad \forall \mathbf{v} \in \mathcal{U}_h. \end{aligned} \tag{3.6e}$$

3.3.2. (F-H-M): Decoupled flow–heat–mechanics

At each iteration all three subproblems are decoupled, and are solved in the order flow → heat → mechanics. This iterative scheme reads: At iteration $k \geq 1$, do:

• **Step 1**: Given $(p^{n,k-1}, T^{n,k-1}, \mathbf{u}^{n,k-1})$ find $(p^{n,k}, \mathbf{w}^{n,k})$ such that

$$\begin{aligned}&(\varphi_{L_p}(T^{n,k-1}, p^{n,k}, \mathbf{u}^{n,k-1}), q) + \tau(\nabla \cdot \mathbf{w}^{n,k}, q)\\ &\quad = \tau(g, q) + (\varphi(T^{n-1}, p^{n-1}, \mathbf{u}^{n-1}), q)\\ &\qquad + L_p(p^{n,k-1}, q), \qquad \forall q \in \mathcal{P}_h, \end{aligned} \tag{3.7a}$$

$$(\mathbf{K}^{-1}\mathbf{w}^{n,k}, \mathbf{z}) - (p^{n,k}, \nabla \cdot \mathbf{z}) = 0, \qquad \forall \mathbf{z} \in \mathcal{W}_h. \tag{3.7b}$$

• **Step 2**: Given $(p^{n,k}, \mathbf{w}^{n,k}, T^{n,k-1}, \mathbf{u}^{n,k-1})$, find $(T^{n,k}, \mathbf{r}^{n,k})$ such that

$$\begin{aligned}&(\psi_{L_T}(T^{n,k}, p^{n,k}, \mathbf{u}^{n,k-1}), S)\\ &\quad + \tau c_f(\mathcal{M}(\mathbf{w}^{n,k}) \cdot \boldsymbol{\Theta}^{-1}\mathcal{M}(\mathbf{r}^{n,k}), S) + \tau(\nabla \cdot \mathbf{r}^{n,k}, S)\\ &\qquad = \tau(h, S) + (\psi(T^{n-1}, p^{n-1}, \mathbf{u}^{n-1}), S)\\ &\qquad\quad + L_T(T^{n,k-1}, S) + b_0(p^{n,k}, S) - \beta(\nabla \mathbf{u}^{n,k-1}, S), \quad \forall S \in \mathcal{T}_h, \end{aligned} \tag{3.7c}$$

$$(\boldsymbol{\Theta}^{-1}\mathbf{r}^{n,k}, \mathbf{y}) - (T^{n,k}, \nabla \cdot \mathbf{y}) = 0, \qquad \forall \mathbf{y} \in \mathcal{R}_h. \tag{3.7d}$$

• **Step 3**: Given $(p^{n,k}, T^{n,k})$, find $\mathbf{u}^{n,k}$ such that

$$\begin{aligned}&2\mu(\boldsymbol{\varepsilon}(\mathbf{u}^{n,k}), \boldsymbol{\varepsilon}(\mathbf{v})) + \lambda(\nabla \cdot \mathbf{u}^{n,k}, \nabla \cdot \mathbf{v})\\ &\quad = (\mathbf{f}^n, \mathbf{v}) + (\beta T^{n,k} + \alpha p^{n,k}, \nabla \cdot \mathbf{v}), \qquad \forall \mathbf{v} \in \mathcal{U}_h. \end{aligned} \tag{3.7e}$$

4. Convergence analysis

The starting point for our analysis is the existence and uniqueness of a solution to (2.3). To this aim, we will make use of the following Lemma (cf. [11]), stating the Lipschitz property of the cut-off operator $\mathcal{M}$:

Lemma 4.1 (*Property of* $\mathcal{M}$). *The "cut-off" operator* $\mathcal{M}$ *defined as in Eq.* (2.2) *is uniformly Lipschitz continuous, i.e.,*

$$\|\mathcal{M}(\boldsymbol{z}_1) - \mathcal{M}(\boldsymbol{z}_2)\|_{(L^\infty(\Omega))^d} \leq \|\boldsymbol{z}_1 - \boldsymbol{z}_2\|_{(L^\infty(\Omega))^d}. \tag{4.1}$$

Thus, we have

$$\left\|\mathcal{M}(\mathbf{w}^n) - \mathcal{M}(\mathbf{w}^{n,k})\right\|_{(L^\infty(\Omega))^d} \leq \left\|\mathbf{w}^n - \mathbf{w}^{n,k}\right\|_{(L^\infty(\Omega))^d}, \tag{4.2a}$$

and

$$\left\|\mathcal{M}(\mathbf{w}^n)\right\|_{(L^\infty(\Omega))^d} \leq M. \tag{4.2b}$$

The proof of the next Theorem is based on showing that the scheme (3.2) is a contraction and then, by applying the Banach fixed-point theorem [48], deduce convergence of the scheme. In what follows, we will frequently use the following polarization and binomial identities:

$$4(u, v) = \|u + v\|^2 - \|u - v\|^2, \quad \text{and} \quad 2(u - v, u) = \|u\|^2 + \|u - v\|^2 - \|v\|^2. \tag{4.3}$$

Finally, we define the difference functions between the solutions at the iteration k and $k-1$ of problem (3.2), respectively as

$$\begin{aligned}(e_T^k, \mathbf{e}_{\mathbf{r}}^k, e_p^k, \mathbf{e}_{\mathbf{w}}^k, \mathbf{e}_{\mathbf{u}}^k) &:= (T^{n,k} - T^{n,k-1}, \mathbf{r}^{n,k} - \mathbf{r}^{n,k-1}, \\ &\quad p^{n,k} - p^{n,k-1}, \mathbf{w}^{n,k} - \mathbf{w}^{n,k-1}, \mathbf{u}^{n,k} - \mathbf{u}^{n,k-1}).\end{aligned} \tag{4.4}$$

Hence, we can state the first of our main results:

Theorem 4.2 (*Convergence of the Monolithic L-scheme* **HFM**)**.** *Assuming* (**A1**)–(**A6**) *holds true, and the time step is small enough, i.e.,*

$$\tau < \frac{2(a_0 - b_0)}{c_f^2 M^2 \left(\frac{k_M}{\theta_m} + 1\right) - \frac{\theta_m}{4c_{\Omega,d}}}. \tag{4.5}$$

Then, the monolithic L-scheme **HFM** *(Algorithm 3.1) defines a contraction satisfying*

$$\begin{aligned}&\left(a_0 - b_0 + \frac{L_T}{2} + \frac{\tau\theta_m}{4c_{\Omega,d}} - \frac{\tau c_f^2 M^2}{2}\left(\frac{k_M}{\theta_m} + 1\right)\right)\left\|e_T^k\right\|^2 + \frac{\tau}{2}\left\|\boldsymbol{e}_{\mathbf{r}}^k\right\|_{\boldsymbol{\Theta}^{-1}}^2 \\ &\quad + \left(c_0 - b_0 + \frac{L_p}{2}\right)\left\|e_p^k\right\|^2 + \tau\left\|\boldsymbol{e}_{\boldsymbol{w}}^k\right\|_{\boldsymbol{K}^{-1}}^2 \\ &\quad + 2\mu\left\|\boldsymbol{\varepsilon}(\boldsymbol{e}_{\boldsymbol{u}}^k)\right\|^2 + \lambda\left\|\nabla\cdot\boldsymbol{e}_{\boldsymbol{u}}^k\right\|^2 \\ &\quad \le \frac{L_T}{2}\left\|e_T^{k-1}\right\|^2 + \frac{L_p}{2}\left\|e_p^{k-1}\right\|^2 + \frac{\tau}{2}\left\|\boldsymbol{e}_{\boldsymbol{w}}^{k-1}\right\|_{\boldsymbol{K}^{-1}}^2.\end{aligned} \tag{4.6}$$

Therefrom, the limit is the unique solution of the problem (2.3).

Remark 4.1 (*Bound on Time Step*)**.** Note that $a_0 - b_0 > 0$ due to (**A4**) and that

$$c_f^2 M^2 \left(\frac{k_M}{\theta_m} + 1\right) - \frac{\theta_m}{4c_{\Omega,d}} > 0, \tag{4.7}$$

by the choice of M sufficiently large (thus, the right hand side of (4.5) is a positive number). If *a priori* bounds on the fluxes are available, and these are small enough such that M can be chosen to yield equality in (4.7), then there is no constraint on the time step.

Proof. We begin by deriving the error equations satisfied by $(e_T^k, \mathbf{e}_{\mathbf{r}}^k, e_p^k, \mathbf{e}_{\mathbf{w}}^k, \mathbf{e}_{\mathbf{u}}^k)$, i.e., subtract Eqs. (3.2) for k from the ones for $k-1$, and obtain

$$\begin{aligned}&(\psi_{L_T}(e_T^k, e_p^k, \mathbf{e}_{\mathbf{u}}^k), S) + \tau(\nabla\cdot\mathbf{e}_{\mathbf{r}}^k, S) \\ &\quad + \tau c_f(\mathcal{M}(\mathbf{w}^{n,k-1})\cdot\boldsymbol{\Theta}^{-1}[\mathcal{M}(\mathbf{r}^{n,k}) - \mathcal{M}(\mathbf{r}^{n,k-1})], S) \\ &\quad + \tau c_f([\mathcal{M}(\mathbf{w}^{n,k-1}) - \mathcal{M}(\mathbf{w}^{n,k-2})]\cdot\boldsymbol{\Theta}^{-1}\mathcal{M}(\mathbf{r}^{n,k}), S) \\ &\quad = L_T(e_T^{k-1}, S), \qquad \forall S \in \mathcal{T}_h,\end{aligned} \tag{4.8a}$$

$$(\boldsymbol{\Theta}^{-1}\mathbf{e}_{\mathbf{r}}^k, \mathbf{y}) - (e_T^k, \nabla\cdot\mathbf{y}) = 0, \qquad \forall \mathbf{y} \in \mathcal{R}_h, \tag{4.8b}$$

$$(\varphi_{L_p}(e_T^k, e_p^k, \mathbf{e}_{\mathbf{u}}^k), q) + \tau(\nabla\cdot\mathbf{e}_{\mathbf{w}}^k, q) = L_p(e_p^{k-1}, q), \qquad \forall q \in \mathcal{P}_h, \tag{4.8c}$$

$$(\mathbf{K}^{-1}\mathbf{e}_{\mathbf{w}}^k, \mathbf{z}) - (e_p^k, \nabla\cdot\mathbf{z}) = 0, \qquad \forall \mathbf{z} \in \mathcal{W}_h, \tag{4.8d}$$

$$\begin{aligned}&2\mu(\boldsymbol{\varepsilon}(\mathbf{e}_{\mathbf{u}}^k), \boldsymbol{\varepsilon}(\mathbf{v})) + \lambda(\nabla\cdot\mathbf{e}_{\mathbf{u}}^k, \nabla\cdot\mathbf{v}) \\ &\quad - (\beta e_T^k + \alpha e_p^k, \nabla\cdot\mathbf{v}) = 0, \qquad \forall \mathbf{v} \in \mathcal{U}_h.\end{aligned} \tag{4.8e}$$

We choose now $S = e_T^k$, $\mathbf{y} = \tau\mathbf{e}_{\mathbf{r}}^k$, $q = e_p^k$, $\mathbf{z} = \tau\mathbf{e}_{\mathbf{w}}^k$, and $\mathbf{v} = \mathbf{e}_{\mathbf{u}}^k$ as test functions in Eqs. (4.8a)–(4.8e), respectively. Then, summing the resulting equations and using the identity (4.3), together with applying the Cauchy–Schwarz and Young inequalities and some algebraic manipulations, we get,

$$\begin{aligned}&\left(a_0 - b_0 + \frac{L_T}{2}\right)\left\|e_T^k\right\|^2 + \tau\left\|\mathbf{e}_{\mathbf{r}}^k\right\|_{\boldsymbol{\Theta}^{-1}}^2 + \left(c_0 - b_0 + \frac{L_p}{2}\right)\left\|e_p^k\right\|^2 \\ &\quad + \tau\left\|\mathbf{e}_{\mathbf{w}}^k\right\|_{\mathbf{K}^{-1}}^2 + 2\mu\left\|\boldsymbol{\varepsilon}(\mathbf{e}_{\mathbf{u}}^k)\right\|^2 + \lambda\left\|\nabla\cdot\mathbf{e}_{\mathbf{u}}^k\right\|^2 \\ &\quad \le \frac{L_T}{2}\left\|e_T^{k-1}\right\|^2 + \frac{L_p}{2}\left\|e_p^{k-1}\right\|^2\end{aligned}$$

$$
\begin{aligned}
&+ \tau c_f \left\| \mathcal{M}(\mathbf{w}^{k-1}) \cdot \boldsymbol{\Theta}^{-1} \mathbf{e}_{\mathbf{r}}^k \right\| \left\| e_T^k \right\| + \tau c_f \left\| \mathbf{e}_{\mathbf{w}}^{k-1} \cdot \boldsymbol{\Theta}^{-1} \mathcal{M}(\mathbf{r}^{k-1}) \right\| \left\| e_T^k \right\|, \\
&\leq \frac{L_T}{2} \left\| e_T^{k-1} \right\|^2 + \frac{L_p}{2} \left\| e_p^{k-1} \right\|^2 + \tau c_f M \left(\frac{\epsilon_1}{2} + \frac{\epsilon_2}{2} \right) \left\| e_T^k \right\|^2 \\
&+ \tau c_f M \frac{1}{2\epsilon_1} \left\| \mathbf{e}_{\mathbf{r}}^k \right\|_{\boldsymbol{\Theta}^{-1}}^2 + \tau c_f M \frac{k_M}{\theta_m} \frac{1}{2\epsilon_2} \left\| \mathbf{e}_{\mathbf{w}}^{k-1} \right\|_{\mathbf{K}^{-1}}^2,
\end{aligned} \tag{4.9}
$$

for any $\epsilon_1, \epsilon_2 > 0$. From Eq. (4.8b), and by Thomas' lemma [49], there exists $\hat{\mathbf{y}} \in \mathcal{R}_h$ and a constant $c_{\Omega,d} > 0$ depending only on the domain and spatial dimension such that $\nabla \cdot \hat{\mathbf{y}} = e_T^k$ with $\left\| \hat{\mathbf{y}} \right\| \leq c_{\Omega,d} \left\| e_T^k \right\|$. Thus, taking $\hat{\mathbf{y}}$ as a test function in (4.8b) we deduce

$$
\begin{aligned}
\left\| e_T^k \right\|^2 = (e_T^k, \nabla \cdot \hat{\mathbf{y}}) &= (\boldsymbol{\Theta}^{-1} \mathbf{e}_{\mathbf{r}}^k, \hat{\mathbf{y}}) \\
&\leq \left\| \mathbf{e}_{\mathbf{r}}^k \right\|_{\boldsymbol{\Theta}^{-1}} \cdot \frac{1}{\sqrt{\theta_m}} \left\| \hat{\mathbf{y}} \right\| \\
&\leq \left\| \mathbf{e}_{\mathbf{r}}^k \right\|_{\boldsymbol{\Theta}^{-1}} \cdot \frac{c_{\Omega,d}}{\sqrt{\theta_m}} \left\| e_T^k \right\|,
\end{aligned} \tag{4.10}
$$

which leads to

$$
\frac{\theta_m}{c_{\Omega,d}} \left\| e_T^k \right\|^2 \leq \left\| \mathbf{e}_{\mathbf{r}}^k \right\|_{\boldsymbol{\Theta}^{-1}}^2. \tag{4.11}
$$

Replacing (4.11) in (4.9) while choosing $\epsilon_1 = c_f M$ and $\epsilon_2 = c_f M k_M / \theta_m$ leads to

$$
\begin{aligned}
&\left(a_0 - b_0 + \frac{L_T}{2} + \frac{\tau \theta_m}{4 c_{\Omega,d}} - \frac{\tau c_f^2 M^2}{2} \left(\frac{k_M}{\theta_m} + 1 \right) \right) \left\| e_T^k \right\|^2 + \frac{\tau}{4} \left\| \mathbf{e}_{\mathbf{r}}^k \right\|_{\boldsymbol{\Theta}^{-1}}^2 \\
&\quad + \left(c_0 - b_0 + \frac{L_p}{2} \right) \left\| e_p^k \right\|^2 + \tau \left\| \mathbf{e}_{\mathbf{w}}^k \right\|_{\mathbf{K}^{-1}}^2 \\
&\quad + 2\mu \left\| \boldsymbol{\varepsilon}(\mathbf{e}_{\mathbf{u}}^k) \right\|^2 + \lambda \left\| \nabla \cdot \mathbf{e}_{\mathbf{u}}^k \right\|^2 \\
&\quad \leq \frac{L_T}{2} \left\| e_T^{k-1} \right\|^2 + \frac{L_p}{2} \left\| e_p^{k-1} \right\|^2 + \frac{\tau}{2} \left\| \mathbf{e}_{\mathbf{w}}^{k-1} \right\|_{\mathbf{K}^{-1}}^2.
\end{aligned} \tag{4.12}
$$

The contraction of the residuals follows if the time step τ satisfies (4.5). This proves the convergence of the monolithic L-scheme. The limit is then the unique solution of (2.3). □

The well-posedness of the discrete variational problem (2.3) is established by Theorem 4.2, where the solution at time t^n, $n \geq 0$, is denoted by $(T^n, \mathbf{r}^n, p^n, \mathbf{w}^n, \mathbf{u}^n)$. Thus, we can now prove the convergence of the decoupled schemes to this solution. We begin with analyzing the partially decoupled schemes, introduced in Section 3.2. To this end, we let the difference functions defined in (4.4) now be the differences between the solutions at the iteration k of problem (3.3), and the solutions to (2.3), i.e.,

$$
(e_T^k, \mathbf{e}_{\mathbf{r}}^k, e_p^k, \mathbf{e}_{\mathbf{w}}^k, \mathbf{e}_{\mathbf{u}}^k) := (T^{n,k} - T^n, \mathbf{r}^{n,k} - \mathbf{r}^n, p^{n,k} - p^n, \mathbf{w}^{n,k} - \mathbf{w}^n, \mathbf{u}^{n,k} - \mathbf{u}^n). \tag{4.13}
$$

The second of our main results is given through:

Theorem 4.3 (*Convergence of the Partially Decoupled Schemes*)**.** *Assuming* (**A1**)–(**A6**) *holds true, the stabilization parameters are such that*

$$
L_p \geq \frac{4\alpha^2}{3(\frac{2\mu}{d} + \lambda)} \quad \text{and} \quad L_T \geq \frac{4\beta^2}{3(\frac{2\mu}{d} + \lambda)}, \tag{4.14}
$$

and the time step satisfies (4.5), then the partially decoupled L-scheme **HF-M** *(Algorithm 3.2.1) is a contraction given by*

$$
\begin{aligned}
&\left(a_0 - b_0 + \frac{L_T}{2} + \frac{\tau \theta_m}{4 c_{\Omega,d}} - \frac{\tau c_f^2 M^2}{2} \left(\frac{k_M}{\theta_m} + 1 \right) \right) \left\| e_T^k \right\|^2 \\
&\quad + \frac{\tau}{4} \left\| \boldsymbol{e}_{\boldsymbol{r}}^k \right\|_{\boldsymbol{\Theta}^{-1}}^2 + \left(c_0 - b_0 + \frac{L_p}{2} \right) \left\| e_p^k \right\|^2 + \tau \left\| \boldsymbol{e}_{\boldsymbol{w}}^k \right\|_{\boldsymbol{K}^{-1}}^2 \\
&\quad \leq \frac{L_T}{2} \left\| e_T^{k-1} \right\|^2 + \frac{L_p}{2} \left\| e_p^{k-1} \right\|^2 + \frac{\tau}{2} \left\| \boldsymbol{e}_{\boldsymbol{w}}^{k-1} \right\|_{\boldsymbol{K}^{-1}}^2.
\end{aligned} \tag{4.15}
$$

Furthermore,

$$
\frac{\mu}{2} \left\| \boldsymbol{\varepsilon}(\boldsymbol{e}_{\boldsymbol{u}}^k) \right\|^2 + \frac{\lambda}{4} \left\| \nabla \cdot \boldsymbol{e}_{\boldsymbol{u}}^k \right\|^2 \leq \frac{2\alpha^2}{3(\frac{2\mu}{d} + \lambda)} \left\| e_p^k \right\|^2 + \frac{2\beta^2}{3(\frac{2\mu}{d} + \lambda)} \left\| e_T^k \right\|^2. \tag{4.16}
$$

Proof. We start by taking the difference of Eqs. (3.3a)–(3.3e) at iteration k with the corresponding equations solved by $(T^n, \mathbf{r}^n, p^n, \mathbf{w}^n, \mathbf{u}^n)$. This leads to the following set of difference equations:

$$
\begin{aligned}
&(\psi_{L_T}(e_T^k, e_p^k, \mathbf{e}_\mathbf{u}^{k-1}), S) + \tau(\nabla\cdot\mathbf{e}_\mathbf{r}^k, S)\\
&\quad + \tau c_f([\mathcal{M}(\mathbf{w}^{n,k-1}) - \mathcal{M}(\mathbf{w}^n)]\cdot\boldsymbol{\Theta}^{-1}\mathbf{r}^n, S)\\
&\quad\quad + \tau c_f(\mathcal{M}(\mathbf{w}^{n,k-1})\cdot\boldsymbol{\Theta}^{-1}[\mathcal{M}(\mathbf{r}^{n,k}) - \mathcal{M}(\mathbf{r}^n)], S)\\
&\quad\quad\quad = L_T(e_T^{k-1}, S), \qquad \forall S\in\mathcal{T}_h, \qquad (4.17a)\\
&(\boldsymbol{\Theta}^{-1}\mathbf{e}_\mathbf{r}^k, \mathbf{y}) - (e_T^k, \nabla\cdot\mathbf{y}) = 0, \qquad \forall\mathbf{y}\in\mathcal{R}_h \qquad (4.17b)\\
&(\varphi_{L_p}(e_T^k, e_p^k, \mathbf{e}_\mathbf{u}^{k-1}), q) + \tau(\nabla\cdot\mathbf{e}_\mathbf{w}^k, q) = L_p(e_p^{k-1}, q), \qquad \forall q\in\mathcal{P}_h, \qquad (4.17c)\\
&(\mathbf{K}^{-1}\mathbf{e}_\mathbf{w}^k, \mathbf{z}) - (e_p^k, \nabla\cdot\mathbf{z}) = 0, \qquad \forall\mathbf{z}\in\mathcal{W}_h, \qquad (4.17d)\\
&2\mu(\boldsymbol{\varepsilon}(\mathbf{e}_\mathbf{u}^k), \boldsymbol{\varepsilon}(\mathbf{v})) + \lambda(\nabla\cdot\mathbf{e}_\mathbf{u}^k, \nabla\cdot\mathbf{v})\\
&\quad - (\alpha e_p^k + \beta e_T^k, \nabla\cdot\mathbf{v}) = 0, \qquad \forall\mathbf{v}\in\mathcal{U}_h. \qquad (4.17e)
\end{aligned}
$$

The aim now is to show a contraction of successive error functions, thereby implying convergence of the sequences $(T^{n,k}, \mathbf{r}^{n,k}, p^{n,k}, \mathbf{w}^{n,k}, \mathbf{u}^{n,k})$ as $k\to\infty$ for $n\geq 1$. Taking as test functions $q = e_p^k$, $\mathbf{z} = \tau\mathbf{e}_\mathbf{w}^k$, $S = e_T^k$, $\mathbf{y} = \tau\mathbf{e}_\mathbf{r}^k$, and $\mathbf{v} = \mathbf{e}_\mathbf{u}^{k-1}$ in (4.17a)–(4.17e), respectively, and adding the resulting equations together leads to

$$
\begin{aligned}
&\left(a_0 + \frac{L_T}{2}\right)\left\|e_T^k\right\|^2 + \frac{L_T}{2}\left\|e_T^k - e_T^{k-1}\right\|^2 + \tau\left\|\mathbf{e}_\mathbf{r}^k\right\|_{\boldsymbol{\Theta}^{-1}}^2\\
&\quad + \left(c_0 + \frac{L_p}{2}\right)\left\|e_p^k\right\|^2 + \frac{L_p}{2}\left\|e_p^k - e_p^{k-1}\right\|^2 + \tau\left\|\mathbf{e}_\mathbf{w}^k\right\|_{\mathbf{K}^{-1}}^2\\
&\quad\quad + 2\mu\frac{1}{4}\left\|\boldsymbol{\varepsilon}(\mathbf{e}_\mathbf{u}^k + \mathbf{e}_\mathbf{u}^{k-1})\right\|^2 + \lambda\frac{1}{4}\left\|\nabla\cdot(\mathbf{e}_\mathbf{u}^k + \mathbf{e}_\mathbf{u}^{k-1})\right\|^2\\
&\quad\quad = \frac{L_T}{2}\left\|e_T^{k-1}\right\|^2 + \frac{L_p}{2}\left\|e_p^{k-1}\right\|^2 + 2b_0(e_T^k, e_p^k)\\
&\quad\quad\quad + 2\mu\frac{1}{4}\left\|\boldsymbol{\varepsilon}(\mathbf{e}_\mathbf{u}^k - \mathbf{e}_\mathbf{u}^{k-1})\right\|^2 + \lambda\frac{1}{4}\left\|\nabla\cdot(\mathbf{e}_\mathbf{u}^k - \mathbf{e}_\mathbf{u}^{k-1})\right\|^2\\
&\quad\quad\quad - \tau c_f([\mathcal{M}(\mathbf{w}^{n,k-1}) - \mathcal{M}(\mathbf{w}^n)]\cdot\boldsymbol{\Theta}^{-1}\mathcal{M}(\mathbf{r}^n), e_T^k)\\
&\quad\quad\quad\quad - \tau c_f(\mathcal{M}(\mathbf{w}^{n,k-1})\cdot\boldsymbol{\Theta}^{-1}[\mathcal{M}(\mathbf{r}^{n,k}) - \mathcal{M}(\mathbf{r}^n)], e_T^k), \qquad (4.18)
\end{aligned}
$$

where we used the identities (4.3). On the other hand, by taking the difference of Eq. (4.17e) at iteration k and $k-1$, testing with $\mathbf{e}_\mathbf{u}^k - \mathbf{e}_\mathbf{u}^{k-1}$, and using the Cauchy–Schwarz inequality we get

$$
\begin{aligned}
&2\mu\left\|\boldsymbol{\varepsilon}(\mathbf{e}_\mathbf{u}^k - \mathbf{e}_\mathbf{u}^{k-1})\right\|^2 + \lambda\left\|\nabla\cdot(\mathbf{e}_\mathbf{u}^k - \mathbf{e}_\mathbf{u}^{k-1})\right\|^2\\
&\quad = \alpha(e_p^k - e_p^{k-1}, \nabla\cdot(\mathbf{e}_\mathbf{u}^k - \mathbf{e}_\mathbf{u}^{k-1})) + \beta(e_T^k - e_T^{k-1}, \nabla\cdot(\mathbf{e}_\mathbf{u}^k - \mathbf{e}_\mathbf{u}^{k-1}))\\
&\quad\quad \leq \left(\alpha\left\|e_p^k - e_p^{k-1}\right\| + \beta\left\|e_T^k - e_T^{k-1}\right\|\right)\left\|\nabla\cdot(\mathbf{e}_\mathbf{u}^k - \mathbf{e}_\mathbf{u}^{k-1})\right\|. \qquad (4.19)
\end{aligned}
$$

Let now $\xi\in(0,1)$ and rewrite the above estimate as

$$
\begin{aligned}
&2\mu\left\|\boldsymbol{\varepsilon}(\mathbf{e}_\mathbf{u}^k - \mathbf{e}_\mathbf{u}^{k-1})\right\|^2 + \lambda\left\|\nabla\cdot(\mathbf{e}_\mathbf{u}^k - \mathbf{e}_\mathbf{u}^{k-1})\right\|^2\\
&\quad \leq \left(\alpha\left\|e_p^k - e_p^{k-1}\right\| + \beta\left\|e_T^k - e_T^{k-1}\right\|\right)\Big(\xi\sqrt{d}\left\|\boldsymbol{\varepsilon}(\mathbf{e}_\mathbf{u}^k - \mathbf{e}_\mathbf{u}^{k-1})\right\|\\
&\quad\quad + (1-\xi)\left\|\nabla\cdot(\mathbf{e}_\mathbf{u}^k - \mathbf{e}_\mathbf{u}^{k-1})\right\|\Big). \qquad (4.20)
\end{aligned}
$$

We now follow [19] and choose $\xi = \dfrac{2\mu}{2\mu + d\lambda}$, which together with the Young inequality yields

$$
\begin{aligned}
&\frac{\mu}{2}\left\|\boldsymbol{\varepsilon}(\mathbf{e}_\mathbf{u}^k - \mathbf{e}_\mathbf{u}^{k-1})\right\|^2 + \frac{\lambda}{4}\left\|\nabla\cdot(\mathbf{e}_\mathbf{u}^k - \mathbf{e}_\mathbf{u}^{k-1})\right\|^2\\
&\quad \leq \frac{2\alpha^2}{3(\frac{2\mu}{d} + \lambda)}\left\|e_p^k - e_p^{k-1}\right\|^2 + \frac{2\beta^2}{3(\frac{2\mu}{d} + \lambda)}\left\|e_T^k - e_T^{k-1}\right\|^2. \qquad (4.21)
\end{aligned}
$$

Combining this with Eq. (4.18) leads to

$$
\begin{aligned}
&(a_0+\frac{L_T}{2})\left\|e_T^k\right\|^2+\left(\frac{L_T}{2}-\frac{2\beta^2}{3(\frac{2\mu}{d}+\lambda)}\right)\left\|e_T^k-e_T^{k-1}\right\|^2+\tau\left\|\mathbf{e}_\mathbf{r}^k\right\|^2_{\boldsymbol{\Theta}^{-1}}\\
&\quad+(c_0+\frac{L_p}{2})\left\|e_p^k\right\|^2+\left(\frac{L_p}{2}-\frac{2\alpha^2}{3(\frac{2\mu}{d}+\lambda)}\right)\left\|e_p^k-e_p^{k-1}\right\|^2+\tau\left\|\mathbf{e}_\mathbf{w}^k\right\|^2_{\mathbf{K}^{-1}}\\
&\quad+\frac{\mu}{2}\left\|\boldsymbol{\varepsilon}(\mathbf{e}_\mathbf{u}^k+\mathbf{e}_\mathbf{u}^{k-1})\right\|^2+\frac{\lambda}{4}\left\|\nabla\cdot(\mathbf{e}_\mathbf{u}^k+\mathbf{e}_\mathbf{u}^{k-1})\right\|^2\\
&\quad\le\frac{L_p}{2}\left\|e_p^{k-1}\right\|^2+\frac{L_T}{2}\left\|e_T^{k-1}\right\|^2+2b_0(e_T^k,e_p^k)\\
&\quad\quad-\tau c_f([\mathcal{M}(\mathbf{w}^{n,k-1})-\mathcal{M}(\mathbf{w}^n)]\cdot\boldsymbol{\Theta}^{-1}\mathcal{M}(\mathbf{r}^n),e_T^k)\\
&\quad\quad-\tau c_f(\mathcal{M}(\mathbf{w}^{n,k-1})\cdot\boldsymbol{\Theta}^{-1}[\mathcal{M}(\mathbf{r}^{n,k})-\mathcal{M}(\mathbf{r}^n)],e_T^k).
\end{aligned}
\tag{4.22}
$$

We thus need to impose some constraints on the stabilization parameters, i.e., $L_p\ge\dfrac{4\alpha^2}{3(\frac{2\mu}{d}+\lambda)}$ and $L_T\ge\dfrac{4\beta^2}{3(\frac{2\mu}{d}+\lambda)}$. With this, we can discard some positive terms on the left hand side of (4.22), and use the Cauchy–Schwarz and Young inequalities, together with the Lipschitz property of $\mathcal{M}$ to obtain

$$
\begin{aligned}
&\left(a_0-b_0+\frac{L_T}{2}-\tau c_f M(\frac{\epsilon_1}{2}+\frac{\epsilon_2}{2})\right)\left\|e_T^k\right\|^2+\tau\left\|\mathbf{e}_\mathbf{r}^k\right\|^2_{\boldsymbol{\Theta}^{-1}}\\
&\quad+\left(c_0-b_0+\frac{L_p}{2}\right)\left\|e_p^k\right\|^2+\tau\left\|\mathbf{e}_\mathbf{w}^k\right\|^2_{\mathbf{K}^{-1}}\\
&\quad\le\frac{L_p}{2}\left\|e_p^{k-1}\right\|^2+\frac{L_T}{2}\left\|e_T^{k-1}\right\|^2\\
&\quad\quad+\tau c_f M\frac{k_M}{\theta_m}\frac{1}{2\epsilon_1}\left\|\mathbf{e}_\mathbf{w}^{k-1}\right\|^2_{\mathbf{K}^{-1}}+\tau c_f M\frac{1}{2\epsilon_2}\left\|\mathbf{e}_\mathbf{r}^k\right\|^2_{\boldsymbol{\Theta}^{-1}},
\end{aligned}
\tag{4.23}
$$

for some $\epsilon_1,\epsilon_2>0$, and where k_M and θ_m are given by (**A1**)–(**A2**). From (4.17b) we obtain in the same way as in (4.11)

$$
\frac{\theta_m}{c_{\Omega,d}}\left\|e_T^k\right\|^2\le\left\|\mathbf{e}_\mathbf{r}^k\right\|^2_{\boldsymbol{\Theta}^{-1}}.
\tag{4.24}
$$

Replacing (4.24) in (4.23) while choosing $\epsilon_1=c_fMk_M/\theta_m$ and $\epsilon_2=c_fM$, we get

$$
\begin{aligned}
&\left(a_0-b_0+\frac{L_T}{2}+\frac{\tau\theta_m}{4c_{\Omega,d}}-\frac{\tau c_f^2M^2}{2}\left(\frac{k_M}{\theta_m}+1\right)\right)\left\|e_T^k\right\|^2+\frac{\tau}{4}\left\|\mathbf{e}_\mathbf{r}^k\right\|^2_{\boldsymbol{\Theta}^{-1}}\\
&\quad+\left(c_0-b_0+\frac{L_p}{2}\right)\left\|e_p^k\right\|^2+\tau\left\|\mathbf{e}_\mathbf{w}^k\right\|^2_{\mathbf{K}^{-1}}\\
&\quad\le\frac{L_p}{2}\left\|e_p^{k-1}\right\|^2+\frac{L_T}{2}\left\|e_T^{k-1}\right\|^2+\frac{\tau}{2}\left\|\mathbf{e}_\mathbf{w}^{k-1}\right\|^2_{\mathbf{K}^{-1}}.
\end{aligned}
\tag{4.25}
$$

Thus, if the time step τ satisfies (4.5), we can write (4.25) as

$$
F^k\le\frac{1}{1+\delta}F^{k-1},
\tag{4.26}
$$

where

$$
F^k:=\frac{L_p}{2}\left\|e_p^k\right\|^2+\frac{L_T}{2}\left\|e_T^k\right\|+\frac{\tau}{4}\left\|\mathbf{e}_\mathbf{w}^k\right\|^2_{\mathbf{K}^{-1}},
\tag{4.27}
$$

and

$$
\delta:=\min\left\{\frac{2}{L_p}(c_0-b_0),\frac{2}{L_T}\left(a_0-b_0+\frac{\tau\theta_m}{4c_{\Omega,d}}-\frac{\tau c_f^2M^2}{2}\left(\frac{k_M}{\theta_m}+1\right)\right),\frac{1}{2}\right\}>0.
\tag{4.28}
$$

Going back to (4.17e), we choose $\mathbf{v}=\mathbf{e}_\mathbf{u}^k$ as test function, which leads to

$$
\begin{aligned}
2\mu\left\|\boldsymbol{\varepsilon}(\mathbf{e}_\mathbf{u}^k)\right\|^2+\lambda\left\|\nabla\cdot\mathbf{e}_\mathbf{u}^k\right\|^2&=\alpha(e_p^k,\nabla\cdot\mathbf{e}_\mathbf{u}^k)+\beta(e_T^k,\nabla\cdot\mathbf{e}_\mathbf{u}^k)\\
&\le(\alpha\left\|e_p^k\right\|+\beta\left\|e_T^k\right\|)\left\|\nabla\cdot\mathbf{e}_\mathbf{u}^k\right\|\\
&\le(\alpha\left\|e_p^k\right\|+\beta\left\|e_T^k\right\|)\left(\xi\sqrt{d}\left\|\boldsymbol{\varepsilon}(\mathbf{e}_\mathbf{u}^k)\right\|+(1-\xi)\left\|\nabla\cdot\mathbf{e}_\mathbf{u}^k\right\|\right),
\end{aligned}
\tag{4.29}
$$

for some $\xi \in (0,1)$. Following the same steps which led to (4.21), and choosing as before $\xi = \dfrac{2\mu}{2\mu + d\lambda}$, we get by the Young inequality

$$\frac{\mu}{2}\left\|\boldsymbol{\varepsilon}(\mathbf{e}_{\mathbf{u}}^k)\right\|^2 + \frac{\lambda}{4}\left\|\nabla\cdot\mathbf{e}_{\mathbf{u}}^k\right\|^2 \leq \frac{2\alpha^2}{3(\frac{2\mu}{d}+\lambda)}\left\|e_p^k\right\|^2 + \frac{2\beta^2}{3(\frac{2\mu}{d}+\lambda)}\left\|e_T^k\right\|^2. \tag{4.30}$$

This shows a contraction of the residuals and therefore completes the proof. □

Remark 4.2 (*The Other Partially Decoupled Schemes*)**.** For the partially decoupled schemes **HM-F** and **FM-H** (Algorithms 3.2.2 and 3.2.3 respectively) the contractions are obtained similarly as for the scheme **HF-M** with minor changes in the convergence rate. The constraint on the time step (4.5) and lower bounds on the stabilization parameters (4.14) remain unchanged.

Before we state the last of our main results, we let the difference functions defined in (4.13) now be the difference between the solutions at the iteration k of problem (3.7) and the solutions to (2.3). The last of our main results then reads:

Corollary 4.3.1 (*Convergence of the Fully Decoupled Algorithms*)**.** *Under the assumptions of Theorem 4.3, the fully decoupled L-scheme* **F-H-M** *(Algorithm 3.3.2) defines a contraction:*

$$\begin{aligned}\left(a_0 - \frac{b_0}{2} + \frac{L_T}{2} + \frac{\tau\theta_m}{4c_{\Omega,d}} - \frac{\tau c_f^2 M^2}{2}\left(\frac{k_M}{\theta_m}+1\right)\right)\left\|e_T^k\right\|^2 \\ + \left(c_0 - b_0 + \frac{L_p}{2}\right)\left\|e_p^k\right\|^2 + \frac{\tau}{2}\left\|\boldsymbol{e}_{\boldsymbol{w}}^k\right\|^2_{\boldsymbol{K}^{-1}} + \frac{\tau}{4}\left\|\boldsymbol{e}_{\boldsymbol{r}}^k\right\|^2_{\boldsymbol{\Theta}^{-1}} \\ \leq \left(\frac{L_T}{2} + \frac{b_0}{2}\right)\left\|e_T^{k-1}\right\|^2 + \frac{L_p}{2}\left\|e_p^{k-1}\right\|^2.\end{aligned} \tag{4.31}$$

Furthermore, the estimate (4.16) holds true.

Proof. We follow the same lines as in the proof of Theorem 4.3 and take the difference of Eqs. (3.7a)–(3.7d), solved by $(T^n, \mathbf{r}^n, p^n, \mathbf{w}^n, \mathbf{u}^n)$, and obtain the difference equations for the fully decoupled scheme **F-H-M**. We then promptly obtain estimate (4.31), from which the contraction is inferred by choosing the stabilization parameters and the time step. The second estimate follows in exactly the same manner. □

Remark 4.3 (*The Fully Decoupled Scheme* **H-F-M**)**.** The contraction (4.31) holds true for Algorithm 3.3.1 by exchanging in there the coefficients in the right-hand side, i.e., $\dfrac{L_p}{2}$ becomes $\dfrac{L_p}{2} + \dfrac{b_0}{2}$ and $\dfrac{L_T}{2} + \dfrac{b_0}{2}$ becomes $\dfrac{L_p}{2}$.

5. Numerical experiments

In the following, we present three numerical test cases using the algorithms from Section 3. The first is a constructed problem, posed on the unit square domain, with prescribed solutions for the temperature, pressure and displacements. Here, we consider five different parameter regimes, exhausting all possibilities of weak/strong coupling between the subproblems, and compare the number of iterations needed for convergence with decreasing mesh sizes for both stabilized and non-stabilized algorithms. Since analytical solutions are available, we present also discretization errors.

Next, we present two implementations of Mandel's problem [50], which is originally a benchmark problem in linear poroelasticity, extended here to nonlinear thermo-poroelasticity. For the original Mandel problem, analytical solutions for the pressure and displacement field are known. Due to the similarity of the thermo-poroelastic equations with the linear Biot's equations, and due to the lack of benchmark problems for thermo-poroelasticity, we choose to use this problem for our second and third numerical test cases. Even though the analytical solutions are no longer valid when including temperature, we have sufficiently weak temperature effects in the first implementation of Mandel's problem that the computed pressure and displacement field matches the (isothermal) analytical solutions. The second implementation of Mandel's problem includes a heat source, which has a significant effect on both the pressure and displacement. Regarding the spatial discretization, we choose the following finite element spaces:

$$\mathcal{R}_h, \mathcal{W}_h := \{\psi \in H(\mathrm{div};\Omega) : \forall K \in \mathcal{X}_h,\ \psi|_K \in \mathbb{RT}_0(K)\}, \tag{5.1a}$$

$$\mathcal{T}_h, \mathcal{P}_h := \{\varphi \in L^2(\Omega) : \forall K \in \mathcal{X}_h,\ \varphi|_K \in \mathbb{P}_0(K)\}, \tag{5.1b}$$

$$\mathcal{U}_h := \{\eta \in (H^1(\Omega))^d : \forall K \in \mathcal{X}_h,\ \eta|_K \in [\mathbb{P}_1(K)]^d\}, \tag{5.1c}$$

where $\mathbb{RT}_0(K)$ denotes the lowest-order Raviart–Thomas finite-dimensional subspace associated with the element $K \in \mathcal{X}_h$, and $\mathbb{P}_l(K)$ is the space of polynomials on $K \in \mathcal{X}_h$ of total degree less than or equal to l. Thus, the spaces $(\mathcal{T}_h, \mathcal{R}_h)$ and $(\mathcal{P}_h, \mathcal{W}_h)$ are the lowest order Raviart–Thomas mixed finite element spaces for the mixed flow and heat flow subproblems,

Table 1
Smooth solution: Parameter regimes for varying strong/weak coupling between subproblems.

	PR1	PR2	PR3	PR4	PR5
α	1.0	0.1	0.1	1.0	0.1
β	1.0	0.1	1.0	0.1	0.1
b_0	1.0	1.0	0.1	0.1	0.1

respectively. Note that both spaces satisfy the condition (2.1), see e.g., [51] for more details on (mixed) finite elements. The vector valued space $\mathcal{U}_h$ is the first order Lagrange finite element space for the mechanics problem. We employ the following stopping criterion for the iterative algorithms, given in terms of the relative and absolute tolerances, aTOL and rTOL, i.e.,

$$\begin{aligned}&\left\|(T^k, \mathbf{r}^k, p^k, \mathbf{w}^k, \mathbf{u}^k) - (T^{k-1}, \mathbf{r}^{k-1}, p^{k-1}, \mathbf{w}^{k-1}, \mathbf{u}^{k-1})\right\| \\ &\qquad \leq \text{aTOL} + \text{rTOL}\left\|(T^k, \mathbf{r}^k, p^k, \mathbf{w}^k, \mathbf{u}^k)\right\|,\end{aligned} \tag{5.2}$$

where we set aTOL $=$ rTOL $= 1e-6$ for all the computations. For the solution of the linear subproblems, we make use of a direct sparse linear solver from the Python library SciPy [52], i.e., `scipy.sparse.linalg.spsolve`. The present approaches can also be combined with iterative solvers adapted to the various subproblems. All numerical tests are implemented in a finite element code written in Python, the complete source code is accessible at https://github.com/matkbrun/FEM.

Remark 5.1 (*Stability*)**.** The discretization defined by (5.1a)–(5.1c) does not satisfy inf–sup stability unless $\mathcal{U}_h$ is chosen as the space of piecewise quadratic polynomials [53]. We employ here a different stabilization strategy, which is iterative coupling using artificial stabilization parameters. Such strategies (e.g., the Fixed Stress Splitting algorithm) have proven very successful for stabilizing problems of poroelasticity [28].

Remark 5.2 (*Parameter Robustness*)**.** We believe that if the differences $c_0 - b_0$ and/or $a_0 - b_0$ are very small, the problem may become difficult to treat. In such cases it can be advantageous to formulate the mechanics problem like the Stokes equations, as done in [54]. However, such an investigation is outside the scope of the present paper. For more details on parameter robustness for the related problem of poroelasticity, see [53,55].

5.1. Test case 1: Example with manufactured solution

As a first test case, we let the domain be a regular triangularization of the unit square, i.e., $\Omega = [0, 1] \times [0, 1] \subset \mathbb{R}^2$, and prescribe the following smooth solutions for the temperature, pressure and displacement:

$$T(x, t) = tx_1(1 - x_1)x_2(1 - x_2), \tag{5.3a}$$

$$p(x, t) = tx_1(1 - x_1)x_2(1 - x_2), \tag{5.3b}$$

$$\mathbf{u}(x, t) = tx_1(1 - x_1)x_2(1 - x_2)[1, 1]^\top, \tag{5.3c}$$

where $x := (x_1, x_2) \in \mathbb{R}^2$, $t \geq 0$. The flux fields are then computed by

$$\mathbf{r} = -\boldsymbol{\Theta}\nabla T, \quad \text{and} \quad \mathbf{w} = -\mathbf{K}\nabla p, \tag{5.3d}$$

while right hand sides, i.e., z, g and $\mathbf{f}$, can be calculated explicitly using Eqs. (1.1a)–(1.1c). We prescribe homogeneous initial conditions and homogeneous Dirichlet boundary conditions, for the temperature, pressure and displacement. All computations are done on a fixed time step, i.e., $\tau = 1.0$, and continued until criterion (5.2) is satisfied.

For the analysis and comparison of our algorithms, we consider dimensionless equations, i.e., all parameters are set to $1.0e-1$, except for the three coupling coefficients $\{\alpha, \beta, b_0\}$, which we vary in order to *weaken/strengthen* the coupling between the three subproblems. In particular, we consider five different parameter regimes, **PR1–PR5**, specified in Table 1:

We also set $a_0 = c_0 = 2b_0$, thus satisfying (**A4**). We emphasize that the parameter regimes **PR1–PR5** are not intended to have any physical meaning, they are only constructed in order to test the convergence properties of the proposed algorithms. Table 2 shows number of iterations needed for convergence using the six algorithms from Sections 3.1, 3.2 and 3.3 for a single time step with decreasing mesh sizes and stabilization parameters chosen according to equality in (4.14).

We see that for the parameter regimes 1, 3 and 4 we have higher iterations numbers than for parameter regimes 2 and 5, for all six algorithms. This is because $L_T \sim \beta^2$ and $L_p \sim \alpha^2$, and larger stabilization results in higher iteration numbers. Furthermore, as expected, the strongly coupled parameter regime (**PR1**) yields the highest iteration numbers, in particular for the algorithms **HF-M**, **H-F-M** and **F-H-M**. Apart from this, the algorithms are performing robustly both with respect to different coupling regimes and decreasing mesh sizes. For comparison we also provide in Table 3 the results without stabilization, i.e., $L_T = L_p = 0$.

Table 2
Smooth solution: Number of iteration with decreasing mesh sizes for parameter regimes PR1–PR5. Stabilization from theory (i.e., L_T and L_p chosen according to equality in (4.14)).

	PR1	PR2	PR3	PR4	PR5	PR1	PR2	PR3	PR4	PR5
h	HFM					HF-M				
1/4	7	3	8	8	3	31	4	11	11	4
1/8	7	3	7	7	3	35	4	13	13	4
1/16	6	3	7	7	3	40	4	13	13	4
1/32	6	3	7	7	3	41	4	13	13	4
1/64	6	3	7	7	3	41	4	13	13	4
h	HM-F					FM-H				
1/4	9	6	8	11	4	9	6	11	8	4
1/8	9	6	7	11	4	9	6	11	7	4
1/16	9	6	7	11	4	9	6	11	7	4
1/32	9	6	7	11	4	9	6	11	7	4
1/64	9	6	7	11	4	9	6	11	7	4
h	H-F-M					F-H-M				
1/4	20	6	11	11	4	20	6	11	11	4
1/8	22	6	12	12	4	22	6	12	12	4
1/16	24	6	13	13	4	24	6	13	13	4
1/32	24	6	13	13	4	24	6	13	13	4
1/64	24	6	13	13	4	24	6	13	13	4

Table 3
Smooth solution: Number of iterations with decreasing mesh sizes for parameter regimes PR1–PR5. No stabilization (i.e., $L_T = L_p = 0$).

	PR1	PR2	PR3	PR4	PR5	PR1	PR2	PR3	PR4	PR5
h	HFM					HF-M				
1/4	3	3	3	3	3	–	4	16	16	4
1/8	3	3	3	3	3	–	4	19	19	4
1/16	3	3	3	3	3	–	4	20	20	4
1/32	3	3	3	3	3	–	4	20	20	4
1/64	3	3	3	3	3	–	4	20	21	4
h	HM-F					FM-H				
1/4	11	6	4	22	4	11	6	21	4	4
1/8	11	6	4	23	4	11	6	23	4	4
1/16	12	6	4	24	4	11	6	24	4	4
1/32	12	6	4	24	4	12	6	24	4	4
1/64	12	6	4	25	4	12	6	24	4	4
h	H-F-M					F-H-M				
1/4	34	6	17	16	4	34	6	16	17	4
1/8	38	5	19	19	4	38	5	19	19	4
1/16	44	5	20	20	4	44	5	20	20	4
1/32	46	5	20	20	4	46	5	20	21	4
1/64	46	5	21	20	4	46	5	20	21	4

We see here that the fully monolithic algorithm (**HFM**) has low iteration counts for all parameter regimes since this is only a linearization scheme, which does not require stabilization (cf. Theorem 4.2). For the two-level (Section 3.2) and three-level (Section 3.3) algorithms, which involves some splitting as well as linearization, we see that iteration counts for different parameter regimes correspond to the various coupling/decoupling of the subproblems present in the algorithms: Splitting of subproblems that are strongly coupled yields high iteration numbers compared to solving the strongly coupled subproblems together. This is in contrast to employing stabilization, which greatly improves the robustness of the algorithms with respect to variations in parameters. For the strongly coupled parameter regime (**PR1**), we even have no convergence for algorithm **HF-M** when no stabilization is applied.

Furthermore, in order to check the robustness of the proposed schemes with respect to the nonlinear coupling, we adjust the coefficient of the convective term, c_f, in order to make this dominate the flow/heat coupling. Table 4 shows the number of iterations needed for convergence when $c_f = 1.0e1$ for both the strongly coupled parameter regime (**PR1**) and the weakly coupled parameter regime (**PR5**). We also compare the results when no stabilization is applied. Note that we here only use a single mesh with $h = 1/16$.

For the weakly coupled parameter regime (**PR5**), there is no difference in iteration numbers between the stabilized and non-stabilized algorithms, even with a dominating nonlinearity. For the strongly coupled parameter regime (**PR1**), the stabilized algorithms have a significantly lower iteration count. This might be due to the fact that the nonlinearity appears as a coupling term.

Table 4
Smooth solution: Number of iterations with strong nonlinear effects, i.e., $c_f = 10$, and mesh size $h = 1/16$.

Parameters	PR1	PR5	PR1	PR5
#	HFM		HF-M	
Non-stabilized	4	4	–	5
Stabilized	7	4	41	5
#	HM-F		FM-H	
Non-stabilized	11	4	10	4
Stabilized	9	4	8	4
#	H-F-M		F-H-M	
Non-stabilized	48	5	36	4
Stabilized	25	5	22	4

Table 5
Smooth solution: Discretization errors using algorithm H-F-M applied on the weakly coupled parameter regime (PR5), and with $c_f = 0.1$. Stabilization from theory. Convergence rate is of first order for all variables, except for that of the displacement which is of second order. We note that these rates are optimal.

h	$e_{h,T}$	r_T	$e_{h,\mathbf{r}}$	$r_{\mathbf{r}}$	$e_{h,p}$	r_p	$e_{h,\mathbf{w}}$	$r_{\mathbf{w}}$	$e_{h,\mathbf{u}}$	$r_{\mathbf{u}}$
1/4	8.5e−3	–	3.5e−3	–	8.5e−3	–	3.5e−3	–	5.6e−3	–
1/8	4.4e−3	1.93	1.8e−3	1.94	4.4e−3	1.93	1.8e−3	1.94	1.4e−3	4.0
1/16	2.2e−3	2.0	9.3e−4	1.94	2.2e−3	2.0	9.3e−4	1.94	3.6e−4	3.89
1/32	1.1e−3	2.0	4.7e−4	1.98	1.1e−3	2.0	4.7e−4	1.98	9.1e−5	3.96
1/64	5.5e−4	2.0	2.3e−4	2.04	5.5e−4	2.0	2.3e−4	2.04	2.3e−5	3.96

Since analytical solutions are available for this problem, we provide also the discretization errors, denoted by $(e_{h,T}, e_{h,\mathbf{r}}, e_{h,p}, e_{h,\mathbf{w}}, e_{h,\mathbf{u}})$, measured in the L^2-norm. Due to almost no variation in discretization errors between the six algorithms and between the different parameter regimes (less than 5%), we provide in Table 5 the discretization errors using algorithm **H-F-M** applied on the weakly coupled parameter regime (**PR5**). We also include the convergence rates, defined by $r_T := e_{h_j,T}/e_{h_{j+1},T}$, and similarly for the other variables.

5.2. Test case 2: Mandel's problem

We refer to [56] for a detailed description of Mandel's problem. Formulas for the analytical pressure and displacements can be found in [44]. We provide here only a brief description. Mandel's problem is posed on a rectangular domain representing a poroelastic slab of extent $2a$ in the horizontal direction, $2b$ in the vertical direction, and infinitely long in the third direction. The poroelastic slab is contained between two rigid plates, where at the initial time a downward force of magnitude $2F$ is applied to the top plate, with an equal but opposite force applied to the bottom plate. The top and bottom boundaries are treated as impermeable, while zero pressure (and temperature) is prescribed at the right and left boundaries. Due to the nature of Mandel's problem, the pressure, temperature and horizontal component of the displacement varies only in the horizontal direction, while the vertical component of the displacement varies only in the vertical direction. From symmetry considerations, it suffices to consider only the top right quarter rectangle, i.e., the computational domain is $[0, a] \times [0, b]$.

We perform now all computations with dimensional equations and realistic choices of physical parameters. In particular, we take mechanics and flow parameters identical to [20], and heat parameters identical to [41]. However, in [41] the flow-heat coupling coefficient b_0 is taken to be identically zero, hence in order to preserve this coupling we instead choose a suitably small number (which satisfies (**A4**)). All parameters are listed in Table 6.

In terms of our previous notation, we now have

$$\mathbf{K} = \mu_f^{-1}\hat{\mathbf{K}},\ a_0 = T_{\text{ref}}^{-1}\hat{a}_0,\ c_f = T_{\text{ref}}^{-1}\hat{c}_f,\ \boldsymbol{\Theta} = T_{\text{ref}}^{-1}\hat{\boldsymbol{\Theta}},\ \mu = \frac{E}{2(1+\nu)} \text{ and } \lambda = \frac{E\nu}{(1+\nu)(1+2\nu)}, \tag{5.4}$$

and the constraints (**A4**) should be understood as $P_{\text{ref}}c_0 - T_{\text{ref}}b_0 > 0$ and $T_{\text{ref}}^{-1}\hat{a}_0 - P_{\text{ref}}b_0 > 0$, respectively. The magnitude of the compressive force is $F = 2 \times 10^8$ Pa m, and the physical dimensions of the quarter rectangle is given by $a = 100$ m and $b = 10$ m, of which we make a regular triangularization. We impose the compressive force as a Dirichlet boundary condition on the top boundary ($x_2 = b$) for the vertical component of the displacement. We denote by n_1 and n_2 the number of subdivisions of the domain in the x_1 and x_2 directions, respectively. For the first implementation of Mandel's problem we prescribe homogeneous boundary conditions and zero source term and initial condition for the heat problem. Fig. 1 shows the solution profiles for the pressure, temperature and displacements for selected time steps, with the analytical (isothermal) solutions for the pressure and displacement included for comparison.

The computed solutions for pressure and displacement matches the analytical solutions, even though the analytical solutions are only valid for the linear isothermal problem. This is because the induced temperature effect in the system is

Table 6
Mandel's problem: Physical parameters are taken from [20,41].

Symbol	Quantity	Value	Unit
E	Bulk modulus	5.94e9	Pa
ν	Poisson's ratio	0.2	–
c_0	Storage coefficient	6.06e−11	Pa^{-1}
α	Biot's coefficient	1.0	–
μ_f	Fluid viscosity	1.0e−3	Pa s
$\hat{\mathbf{K}}$	Permeability	9.87e−14 $\mathbf{I}$	m^2
$\hat{\boldsymbol{\Theta}}$	Effective thermal conductivity	1.7 $\mathbf{I}$	$\mathrm{W\ m^{-1}\ K^{-1}}$
b_0	Thermal dilation coefficient	3.03e−11	K^{-1}
β	Thermal stress coefficient	9.9e6	$\mathrm{Pa\ K^{-1}}$
$\hat{a}_0$	Effective volumetric heat capacity	0.92e3	$\mathrm{J\ m^{-3}\ K^{-1}}$
T_{ref}	Reference temperature	298.15	K
P_{ref}	Reference pressure	2.0e6	Pa
$\hat{c}_f$	Volumetric heat capacity fluid	4.18e6	$\mathrm{J\ m^{-3}\ K^{-1}}$
τ	Time step	10	s

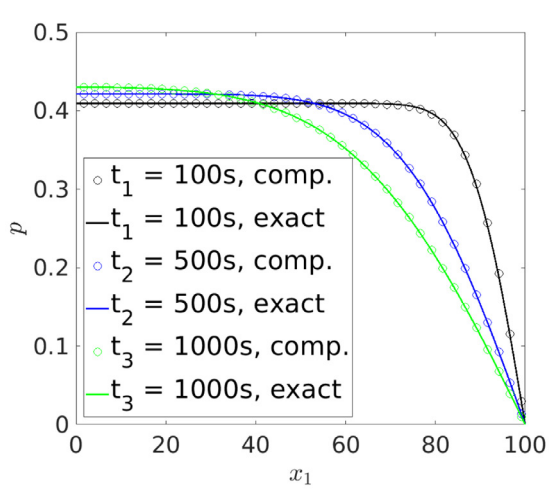

(a) Pressure profile.

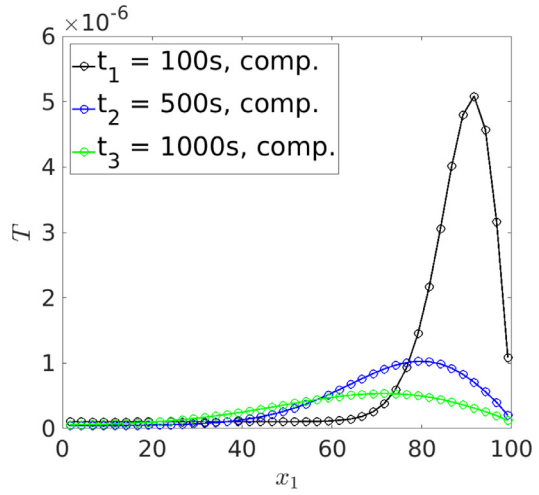

(b) Temperature profile.

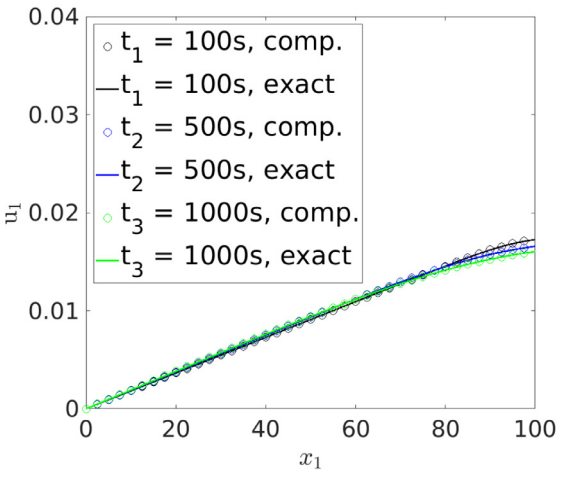

(c) Displacement profile, 1st component.

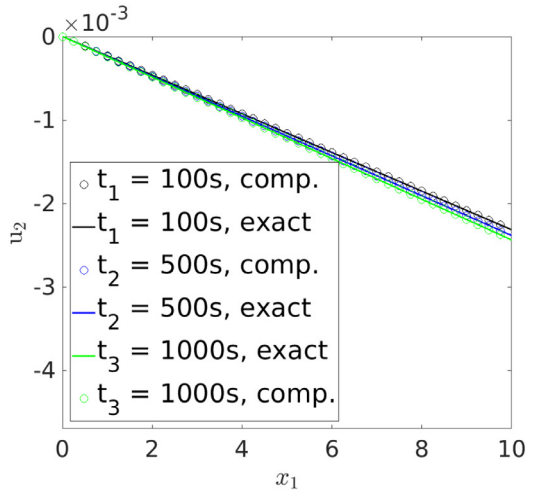

(d) Displacement profile, 2nd component.

Fig. 1. Mandel's problem: Solution profiles for Mandel's problem at $t \in \{100\,\mathrm{s}, 500\,\mathrm{s}, 1000\,\mathrm{s}\}$, computed using the monolithic scheme **HFM**, with $z = 0\ \mathrm{W\ m^{-3}\ K^{-1}}$, and $n_1 = n_2 = 40$.

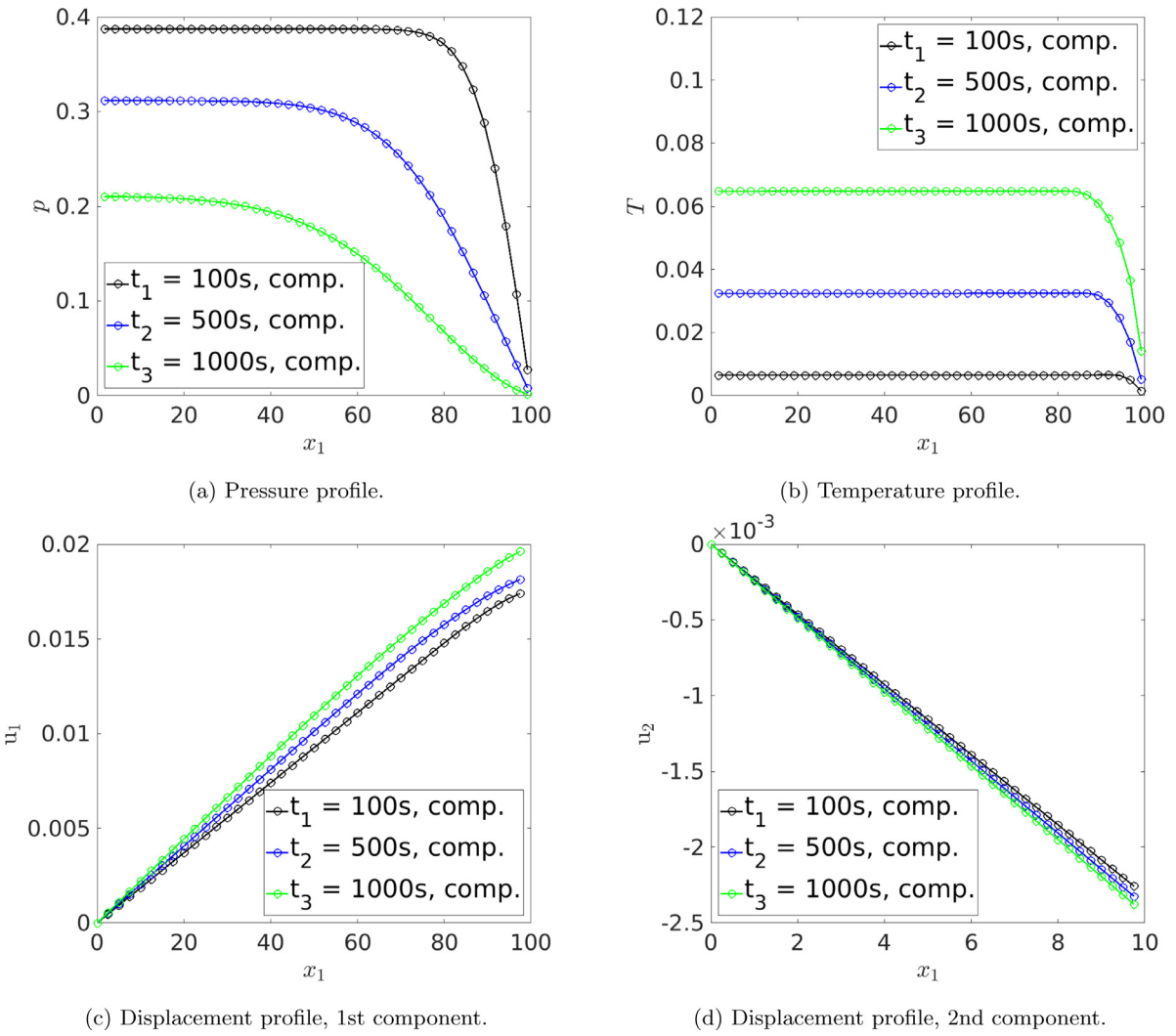

(a) Pressure profile.

(b) Temperature profile.

(c) Displacement profile, 1st component.

(d) Displacement profile, 2nd component.

Fig. 2. Mandel's problem: Solution profiles at $t \in \{100\,\text{s}, 500\,\text{s}, 1000\,\text{s}\}$, computed using the monolithic scheme **HFM**, with $z = 2 \times 10^{-4}$ W m^{-3} K^{-1}, and $n_1 = n_2 = 40$.

Table 7
Mandel's problem: Number of iterations with decreasing mesh sizes for Mandel's problem. Stabilization from theory.

Heat source	$z = 0$	$z = 2\text{e}{-4}$	$z = 0$	$z = 2\text{e}{-4}$	$z = 0$	$z = 2\text{e}{-4}$
$n_1 = n_2$	HFM		HF–M		HM–F	
10	18	18	14	14	14	14
20	18	18	13	12	13	12
40	18	18	13	12	13	12
$n_1 = n_2$	FM–H		H–F–M		F–H–M	
10	18	18	14	13	14	14
20	18	18	13	13	13	12
40	18	18	13	13	13	12

small enough that the heat decouples from the flow and mechanics. For the second implementation of Mandel's problem we prescribe a constant source term for the heat problem, i.e., $z = 2 \times 10^{-4}$ W m^{-3} K^{-1} and zero initial condition. Fig. 2 shows the solution profiles for the pressure, temperature and displacements at selected time steps.

The temperature source now interacts with the other processes and thus has an effect on the pressure and horizontal component of the displacement. Furthermore, the temperature change in the system is now increasing with increasing time. Table 7 shows the number of iterations for Mandel's problem using the derived algorithms.

6. Conclusions

Based on previous developments of iterative splitting schemes from linear poroelasticity, we have proposed six novel iterative procedures for nonlinear thermo-poroelasticity. These algorithms are using stabilization and linearization techniques similar to [19,34], which is known in the literature as the '*L*-scheme'. The thermo-poroelastic problem we consider can be viewed as a coupling of three physical processes (or subproblems): Flow, geomechanics and heat. Solving this system either monolithically (all three subproblems simultaneously), partially decoupled (two subproblems simultaneously), or fully decoupled (each subproblem separately), yields six possible combinations of coupling/decoupling, which we have used to design our six algorithms. All of these involve a linearization of the convective term and added stabilization terms to both the flow and heat subproblems. In this sense, our use of the *L*-scheme is both as a stabilization for iterative splitting and a linearization of nonlinear problems.

For any given situation, the coupling strength between the three subproblems may vary. A-priori, the expectation is that solving together subproblems that are strongly coupled yields better efficiency and accuracy than splitting strategies. On the other hand, if the coupling between two or more subproblems is weak, a splitting procedure might be beneficial. For this reason, and due to the fact that splitting the three-way coupled multi-physics problem into smaller subproblems allows for combining existing codes that separately can handle any of the three processes involved (or two of them combined), six different algorithms are presented. These six algorithms cover all possibilities of strong/weak coupling between the three subproblems. Using the well-posedness of the continuous problem, we obtained lower bounds on the stabilization parameters and proved the convergence of our proposed algorithms under a constraint on the time step. In practice, however, we find that this bound is not tight; as long as the fluxes are not becoming unbounded (e.g., due to a singularity), a 'reasonable' time step can safely be chosen.

Our algorithms are tested in detail with several numerical examples. In particular, we find that all six algorithms are performing robustly with respect to both mesh refinement and different parameter regimes (i.e., strong/weak coupling between the subproblems and strong/weak nonlinear effects), using the stabilization revealed by our analysis. We also find that using no stabilization results in the algorithms being more sensitive to the parameter regimes, i.e., splitting subproblems that are strongly coupled yields high iteration numbers compared to solving these subproblems together. This phenomenon is also observed in the stabilized algorithms, but to a significantly lesser extent. In particular, our conclusion is that with no stabilization, each of the algorithms is suitable only for a certain parameter regime (i.e., one that corresponds to the coupling/decoupling structure present in the algorithm). This is in contrast to the stabilized algorithms, which can handle a much wider range of different parameter regimes.

CRediT authorship contribution statement

Mats Kirkesæther Brun: Conceptualization, Methodology, Derivation, Software and coding. **Elyes Ahmed:** Conceptualization, Methodology, Derivation. **Inga Berre:** Conceptualization, Methodology, Derivation. **Jan Martin Nordbotten:** Conceptualization, Methodology, Derivation. **Florin Adrian Radu:** Conceptualization, Methodology, Derivation.

Acknowledgment

The research is supported by the Norwegian Research Council Toppforsk project 250223 (The TheMSES project: https://themses.w.uib.no), and the University of Bergen, Norway.

References

[1] K. Terzaghi, Theoretical Soil Mechanics, Chapman And Hali, Limited John Wiley And Sons, Inc., New York, 1944, http://dx.doi.org/10.1002/9780470172766.
[2] M.A. Biot, General theory of three-dimensional consolidation, J. Appl. Phys. 12 (1941) 155–164, http://dx.doi.org/10.1063/1.1712886.
[3] M.A. Biot, G. Temple, Theory of finite deformations of porous solids, Indiana Univ. Math. J. 21 (1972) 597–620, http://www.jstor.org/stable/24890361.
[4] M.K. Brun, I. Berre, J.M. Nordbotten, F.A. Radu, Upscaling of the coupling of hydromechanical and thermal processes in a quasi-static poroelastic medium, Transp. Porous Media (2018) http://dx.doi.org/10.1007/s11242-018-1056-8.
[5] C.K. Lee, C.C. Mei, Thermal consolidation in porous media by homogenization theory—i. derivation of macroscale equations, Adv. Water Resour. 20 (1997) 127–144, http://dx.doi.org/10.1016/S0309-1708(96)00026-7.
[6] C.J. van Duijn, A. Mikelić, M.F. Wheeler, T. Wick, Thermoporoelasticity via homogenization: modeling and formal two-scale expansions, Internat. J. Engrg. Sci. 138 (2019) 1–25, http://dx.doi.org/10.1016/j.ijengsci.2019.02.005.
[7] B. Gatmiri, P. Delage, A formulation of fully coupled thermal–hydraulic–mechanical behaviour of saturated porous media—numerical approach, Int. J. Numer. Anal. Methods Geomech. 21 (1997) 199–225, http://dx.doi.org/10.1002/(SICI)1096-9853(199703)21:3<199::AID-NAG865>3.0.CO;2-M.
[8] A.P. Suvorov, A.P.S. Selvadurai, Macroscopic constitutive equations of thermo-poroviscoelasticity derived using eigenstrains, J. Mech. Phys. Solids 58 (2010) 1461–1473, http://dx.doi.org/10.1016/j.jmps.2010.07.016.
[9] U. Hornung, Homogenization and Porous Media, vol. 6, Springer Science & Business Media, 2012, http://dx.doi.org/10.1007/978-1-4612-1920-0.
[10] S. Sun, B. Rivière, M.F. Wheeler, A combined mixed finite element and discontinuous Galerkin method for miscible displacement problem in porous media, in: Recent Progress in Computational and Applied PDEs (Zhangjiajie, 2001), Kluwer/Plenum, New York, 2002, pp. 323–351.
[11] S. Sun, M.F. Wheeler, Discontinuous Galerkin methods for coupled flow and reactive transport problems, Appl. Numer. Math. 52 (2005) 273–298, http://dx.doi.org/10.1016/j.apnum.2004.08.035.

[12] M.K. Brun, E. Ahmed, J.M. Nordbotten, F.A. Radu, Well-posedness of the fully coupled quasi-static thermo-poroelastic equations with nonlinear convective transport, J. Math. Anal. Appl. 471 (2019) 239–266, http://dx.doi.org/10.1016/j.jmaa.2018.10.074.
[13] C. Chainais-Hillairet, J. Droniou, Convergence analysis of a mixed finite volume scheme for an elliptic–parabolic system modeling miscible fluid flows in porous media, SIAM J. Numer. Anal. 45 (2007) 2228–2258, http://dx.doi.org/10.1137/060657236.
[14] B. a. da Veiga, J. Droniou, G. Manzini, A unified approach for handling convection terms in finite volumes and mimetic discretization methods for elliptic problems, IMA J. Numer. Anal. 31 (2011) 1357–1401, http://dx.doi.org/10.1093/imanum/drq018.
[15] E. Ahmed, F.A. Radu, J.M. Nordbotten, Adaptive poromechanics computations based on a posteriori error estimates for fully mixed formulations of Biot's consolidation model, Comput. Methods Appl. Mech. Engrg. 347 (2019) 264–294, http://dx.doi.org/10.1016/j.cma.2018.12.016.
[16] C.N. Dawson, H. Klíe, M.F. Wheeler, C.S. Woodward, A parallel, implicit, cell-centered method for two-phase flow with a preconditioned Newton-Krylov solver, Comput. Geosci. 1 (1997) (1998) 215–249, http://dx.doi.org/10.1023/A:1011521413158.
[17] M.A. Fernández, J.-F. Gerbeau, C. Grandmont, A projection semi-implicit scheme for the coupling of an elastic structure with an incompressible fluid, Internat. J. Numer. Methods Engrg. 69 (2007) 794–821, http://dx.doi.org/10.1002/nme.1792.
[18] S.E. Minkoff, C. Stone, S. Bryant, M. Peszynska, M.F. Wheeler, Coupled fluid flow and geomechanical deformation modeling, J. Petrol. Sci. Eng. 38 (2003) 37–56, http://dx.doi.org/10.1016/S0920-4105(03)00021-4, http://www.sciencedirect.com/science/article/pii/S0920410503000214.
[19] J.W. Both, M. Borregales, J.M. Nordbotten, K. Kumar, F.A. Radu, Robust fixed stress splitting for Biot's equations in heterogeneous media, Appl. Math. Lett. 68 (2017) 101–108, http://dx.doi.org/10.1016/j.aml.2016.12.019.
[20] A. Mikelić, B. Wang, M.F. Wheeler, Numerical convergence study of iterative coupling for coupled flow and geomechanics, Comput. Geosci. 18 (2014) 325–341, http://dx.doi.org/10.1007/s10596-013-9393-8.
[21] N. Castelletto, J. White, H. Tchelepi, A unified framework for fully-implicit and sequential-implicit schemes for coupled poroelasticity, in ECMOR XIV-14th European Conference on the Mathematics of Oil Recovery, 2014, http://dx.doi.org/10.3997/2214-4609.20141897.
[22] J.G. Garcia, L.W. Teufel, et al., Numerical simulation of fully coupled fluid-flow/geomechanical deformation in hydraulically fractured reservoirs, in: SPE Production Operations Symposium, Society of Petroleum Engineers, 2005, http://dx.doi.org/10.2118/94062-MS.
[23] J.A. White, N. Castelletto, H.A. Tchelepi, Block-partitioned solvers for coupled poromechanics: a unified framework, Comput. Methods Appl. Mech. Engrg. 303 (2016) 55–74, http://dx.doi.org/10.1016/j.cma.2016.01.008.
[24] M. Bukač, I. Yotov, P. Zunino, An operator splitting approach for the interaction between a fluid and a multilayered poroelastic structure, Numer. Methods Partial Differential Equations 31 (2015) 1054–1100, http://dx.doi.org/10.1002/num.21936.
[25] E. Ahmed, J. Jaffré, J.E. Roberts, A reduced fracture model for two-phase flow with different rock types, Math. Comput. Simulation 137 (2017) 49–70, http://dx.doi.org/10.1016/j.matcom.2016.10.005.
[26] D. Néron, D. Dureisseix, A computational strategy for thermo-poroelastic structures with a time-space interface coupling, Internat. J. Numer. Methods Engrg. 75 (2008) 1053–1084, http://dx.doi.org/10.1002/nme.2283.
[27] E. Ahmed, J.M. Nordbotten, F.A. Radu, Adaptive asynchronous time-stepping, stopping criteria, and a posteriori error estimates for fixed-stress iterative schemes for coupled poromechanics problems, J. Comput. Appl. Math. 364 (2020) 112312, 25, http://dx.doi.org/10.1016/j.cam.2019.06.028.
[28] N. Castelletto, J. White, H. Tchelepi, Accuracy and convergence properties of the fixed-stress iterative solution of two-way coupled poromechanics, Int. J. Numer. Anal. Methods Geomech. 39 (2015) 1593–1618, http://dx.doi.org/10.1002/nag.2400.
[29] O. Iliev, A. Kolesov, P. Vabishchevich, Numerical solution of plate poroelasticity problems, Transp. Porous Media 115 (2016) 563–580, http://dx.doi.org/10.1007/s11242-016-0726-7.
[30] J. Kim, H.A. Tchelepi, R. Juanes, et al., Stability, accuracy and efficiency of sequential methods for coupled flow and geomechanics, in: SPE Reservoir Simulation Symposium, Society of Petroleum Engineers, 2009, http://dx.doi.org/10.2118/119084-MS.
[31] A.E. Kolesov, P.N. Vabishchevich, Splitting schemes with respect to physical processes for double-porosity poroelasticity problems, Russian J. Numer. Anal. Math. Modelling 32 (2017) 99–113, http://dx.doi.org/10.1515/rnam-2017-0009.
[32] A. Mikelić, M.F. Wheeler, Convergence of iterative coupling for coupled flow and geomechanics, Comput. Geosci. 17 (2013) 455–461, http://dx.doi.org/10.1007/s10596-012-9318-y.
[33] D. Tran, L. Nghiem, L. Buchanan, et al., An overview of iterative coupling between geomechanical deformation and reservoir flow, in: SPE International Thermal Operations and Heavy Oil Symposium, Society of Petroleum Engineers, 2005, http://dx.doi.org/10.2118/97879-MS.
[34] F. List, F.A. Radu, A study on iterative methods for solving Richards' equation, Comput. Geosci. 20 (2016) 341–353, http://dx.doi.org/10.1007/s10596-016-9566-3.
[35] I.S. Pop, F. Radu, P. Knabner, Mixed finite elements for the Richards' equation: linearization procedure, J. Comput. Appl. Math. 168 (2004) 365–373, http://dx.doi.org/10.1016/j.cam.2003.04.008.
[36] M. Borregales, F.A. Radu, K. Kumar, J.M. Nordbotten, Robust iterative schemes for non-linear poromechanics, Comput. Geosci. 22 (2018) 1021–1038, http://dx.doi.org/10.1007/s10596-018-9736-6.
[37] J.W. Both, K. Kumar, J.M. Nordbotten, F.A. Radu, Anderson accelerated fixed-stress splitting schemes for consolidation of unsaturated porous media, Comput. Math. Appl. 77 (2019) 1479–1502, http://dx.doi.org/10.1016/j.camwa.2018.07.033.
[38] V. Dolejší, M. Kuraz, P. Solin, Adaptive higher-order space–time discontinuous Galerkin method for the computer simulation of variably-saturated porous media flows, Appl. Math. Model. 72 (2019) 276–305, http://dx.doi.org/10.1016/j.apm.2019.02.037.
[39] F.A. Radu, J.M. Nordbotten, I.S. Pop, K. Kumar, A robust linearization scheme for finite volume based discretizations for simulation of two-phase flow in porous media, J. Comput. Appl. Math. 289 (2015) 134–141, http://dx.doi.org/10.1016/j.cam.2015.02.051.
[40] K. Mitra, I.S. Pop, A modified L-scheme to solve nonlinear diffusion problems, Comput. Math. Appl. 77 (2019) 1722–1738, http://dx.doi.org/10.1016/j.camwa.2018.09.042.
[41] J. Kim, Unconditionally stable sequential schemes for all-way coupled thermoporomechanics: undrained-adiabatic and extended fixed-stress splits, Comput. Methods Appl. Mech. Engrg. 341 (2018) 93–112, http://dx.doi.org/10.1016/j.cma.2018.06.030.
[42] A.E. Kolesov, P.N. Vabishchevich, M.V. Vasilyeva, Splitting schemes for poroelasticity and thermoelasticity problems, Comput. Math. Appl. 67 (2014) 2185–2198, http://dx.doi.org/10.1016/j.camwa.2014.02.005.
[43] D. Seus, K. Mitra, I.S. Pop, F.A. Radu, C. Rohde, A linear domain decomposition method for partially saturated flow in porous media, Comput. Methods Appl. Mech. Engrg. 333 (2018) 331–355, http://dx.doi.org/10.1016/j.cma.2018.01.029.
[44] P.J. Phillips, M.F. Wheeler, A coupling of mixed and discontinuous Galerkin finite-element methods for poroelasticity, Comput. Geosci. 12 (2008) 417–435, http://dx.doi.org/10.1007/s10596-008-9082-1.
[45] S.-Y. Yi, Convergence analysis of a new mixed finite element method for Biot's consolidation model, Numer. Methods Partial Differential Equations 30 (2014) 1189–1210, http://dx.doi.org/10.1002/num.21865.
[46] I. Ambartsumyan, E. Khattatov, T. Nguyen, I. Yotov, Flow and transport in fractured poroelastic media, GEM Int. J. Geomath. 10 (2019) Art. 11, 34, http://dx.doi.org/10.1007/s13137-019-0119-5.
[47] F. Doster, J.M. Nordbotten, et al., Full pressure coupling for geo-mechanical multi-phase multi-component flow simulations, in: SPE Reservoir Simulation Symposium, Society of Petroleum Engineers, 2015, http://dx.doi.org/10.2118/173232-MS.
[48] W. Cheney, Analysis for Applied Mathematics, in: Graduate Texts in Mathematics, vol. 208, Springer-Verlag, New York, 2001, http://dx.doi.org/10.1007/978-1-4757-3559-8.

[49] J.M. Thomas, Méthode des éléments finis équilibre, in: Journées éléments Finis (Rennes, 1975), Univ. Rennes, Rennes, 1975, p. 25, http://eudml.org/doc/273740.
[50] J. Mandel, Consolidation des sols (étude mathématique), Geotechnique 3 (1953) 287–299, http://dx.doi.org/10.1680/geot.1953.3.7.287.
[51] G.N. Gatica, A simple introduction to the mixed finite element method, in: Theory and Applications, in: Springer Briefs in Mathematics, Springer, London, 2014, http://dx.doi.org/10.1007/978-3-319-03695-3.
[52] T.E. Oliphant, Python for scientific computing, Comput. Sci. Eng. 9 (2007) 10–20, http://dx.doi.org/10.1109/MCSE.2007.58.
[53] Q. Hong, J. Kraus, Parameter-robust stability of classical three-field formulation of Biot's consolidation model, Electron. Trans. Numer. Anal. 48 (2018) 202–226, http://dx.doi.org/10.1553/etna_vol48s202.
[54] J.J. Lee, K.-A. Mardal, R. Winther, Parameter-robust discretization and preconditioning of Biot's consolidation model, SIAM J. Sci. Comput. 39 (2017) A1–A24, http://dx.doi.org/10.1137/15M1029473.
[55] Q. Hong, J. Kraus, M. Lymbery, F. Philo, Conservative discretizations and parameter-robust preconditioners for biot and multiple-network flux-based poroelasticity models, Numer. Linear Algebra Appl. 26 (2019) e2242, http://dx.doi.org/10.1002/nla.2242.
[56] O. Coussy, Poromechanics, John Wiley & Sons, 2004, http://dx.doi.org/10.1002/0470092718.